NASA CR-73366

AVAILABLE TO THE PUBLIC

APPLICATION OF THE VARIATIONAL STEEPEST-DESCENT METHOD TO HIGH PERFORMANCE AIRCRAFT TRAJECTORY OPTIMIZATION

By Donald S. Hague

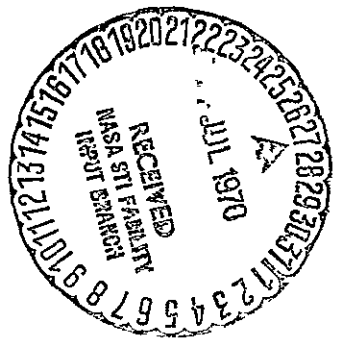

Prepared Under Contract NAS 2-5383
AEROPHYSICS RESEARCH CORPORATION
Box 187,Bellevue, Wash.

For

AMES RESEARCH CENTER, MOFFETT FIELD, CALIFORNIA
NATIONAL AERONAUTICS AND SPACE ADMINISTRATION

NASA CR-73366

APPLICATION OF THE VARIATIONAL STEEPEST-DESCENT METHOD TO HIGH PERFORMANCE AIRCRAFT TRAJECTORY OPTIMIZATION

By Donald S. Hague

Prepared Under Contract NAS 2-5383
AEROPHYSICS RESEARCH CORPORATION
Box 187,Bellevue, Wash.

For

AMES RESEARCH CENTER, MOFFETT FIELD, CALIFORNIA
NATIONAL AERONAUTICS AND SPACE ADMINISTRATION

PREFACE

This document reports a study carried out by Aerophysics Research Corporation during the period from April to August 1969, under Contract NAS 2-4507. The National Aeronautics and Space Administration Technical Monitor was Mr. Richard H. Petersen, Mission Analysis Division, Moffett Field, California. Mr. D. S. Hague functioned as Aerophysics Research Corporation Project Leader for the study.

The trajectory program and steepest-descent optimization program employed in the study were originally developed under U. S. Air Force funding Contacts AF 33(616)-6848 and AF 33 (657)-8829. Mr. B. R. Benson of the Air Force Flight Dynamics Laboratory sponsored these developments. The optimization program was further extended under NASA Contract NAS 2-3691. Mr. Hubert Drake of the Mission Analysis Division, Moffett Field, California monitored that study.

Mrs. Margaret King and Mrs. Natalie James of the Ames Research Center provided programming and operational support in setting up the optimization program on the ARC IBM 7040/ 7094 DCS Digital Computer System. Mr. Mark Ardema, Mr. Mark Waters and Mr. Lew Williams of the Mission Analysis Division assisted in the data preparation for the vehicles employed in the study.

TABLE OF CONTENTS

LIST OF FIGURES

LIST OF FIGURES (Continued)

LIST OF FIGURES (Continued)

APPLICATION OF THE VARIATIONAL STEEPEST-DESCENT METHOD TO HIGH PERFORMANCE AIRCRAFT TRAJECTORY OPTIMIZATION

by Donald S. Hague
Aerophysics Research Corporation

SUMMARY

The variational steepest-descent method is applied to a variety of aircraft and aircraft performance problems. Vehicle types employed in the calculations consist of a typical next-generation Hypersonic Research Aircraft and a Supersonic Transport configuration.

Performance problems considered include minimum time-to-climb, minimum fuel ascents, maximum range, and minimum range (the return to base problem). Solutions are obtained for a variety of terminal constraints including velocity, altitude, and flight path angle. In several cases, in-flight inequality constraints are imposed on vehicle state and control functions including maximum altitude, throttle setting, acceleration, and flight path angle. The inequality constraints are imposed either separately or in combination. Control variables employed include angle-of-attack, pitch angle, bank-angle, and throttle setting. Convergence to the optimal solution is obtained automatically by a second-order step-size criteria in combination with "artificial intelligence" in the form of programmed logical decisions.

The program employed was subject to the limitations of a single vehicle (or at most two vehicles, one of which is in a prespecified circular planetary orbit) and to employment of stages at fixed times.

HYPERSONIC RESEARCH AIRCRAFT ASCENT TRAJECTORIES

The trajectory optimization program described in detail in References 1 through 3 was applied to selected performance problems for a possible Hypersonic Research Aircraft (HRA). This vehicle is being studied by NASA personnel at the Mission Analysis Division. Optimal trajectories were first derived with operational constraints removed. These trajectories, then, provide upper bounds on vehicle performance. Where feasible in the time span of the present study, operational constraints were subsequently introduced one at a time, and the trajectories were re-optimized. In this manner, the performance cost associated with each constraint can be clearly recognized.

Since study objectives include a demonstration of the ability of steepest-descent methods in solution of HRA performance optimization problems, no attempt to determine "good" starting points was undertaken. Rather, straightforward ramped or constant value control histories were employed for nominal flight path generation. In certain cases solutions were obtained from more than one starting point in order to verify convergence to a single, distinct optimal path. These calculations successfully demonstrated such convergence behavior. In the calculations angle-of-attack control was employed in the vertical plane except where otherwise stated. A trajectory optimization calculation performed by NASA personnel employing a version of the parameter optimization and vehicle analysis program of References 4 to 8 is also included for comparison purposes.

Vehicle Characteristics

Hypersonic Research Aircraft vehicle characteristics and flight path for ascent to level flight at Mach 12 at 119300 feet were optimized by NASA personnel prior to commencement of the present study. Initial conditions correspond to horizontal take-off at the altitude of Edwards Air Force Base (2300 feet). Design optimization was accomplished by means of an extended version of the program of References 4 to 6. An outline of the resulting vehicle is presented in Figure 1 and the ascent trajectory profile to which the vehicle is optimized is shown in Figure 2. As noted in Reference 6 the trajectory equations of the program utilized in design optimization studies are approximate ones, notably, the $\dot{\gamma}$ terms are ignored in the vehicle equations of motion. Hence, the trajectories obtained in the present study using the complete equations of motion contained in the program of References 1 and 2 permit assessment of the error involved in the use of approximate flight path equations of motion.

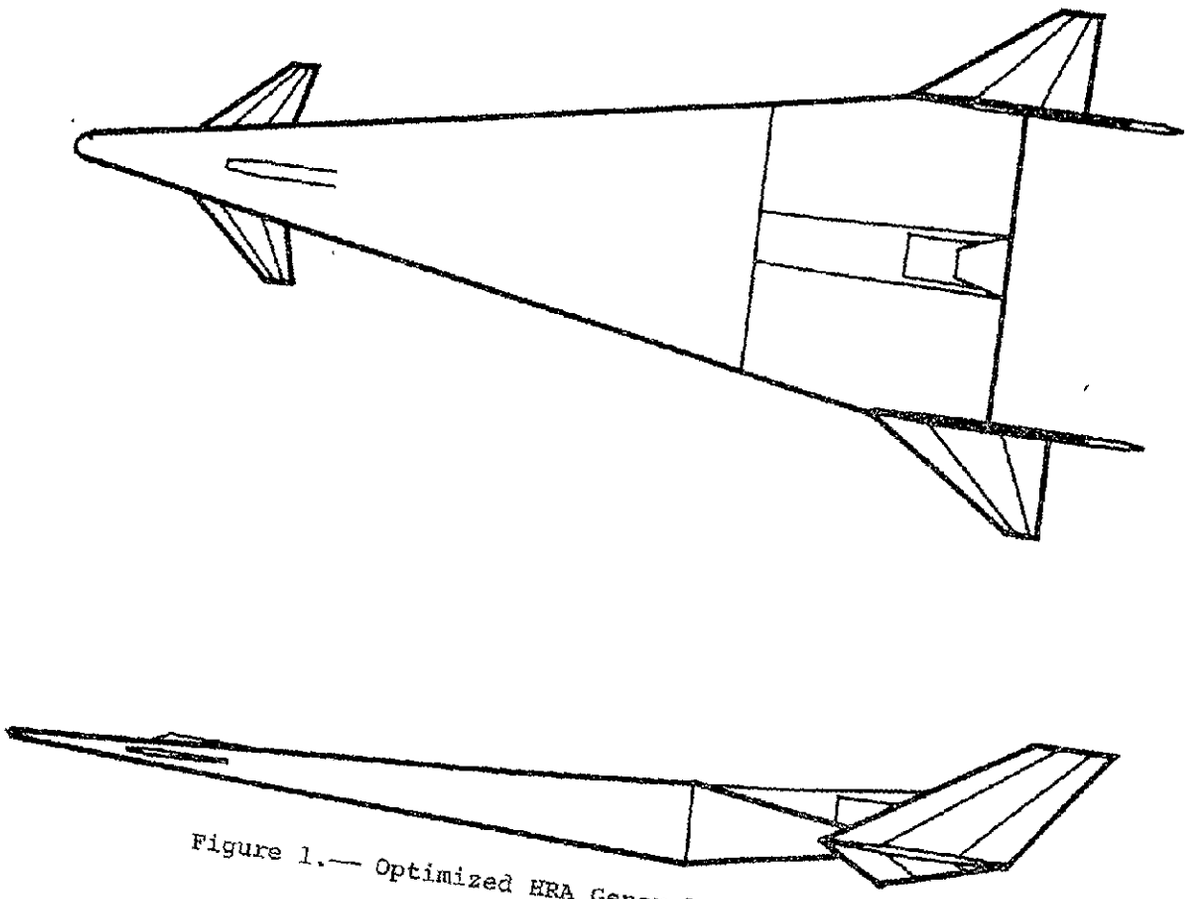

Figure 1.— Optimized HRA General Arrangement

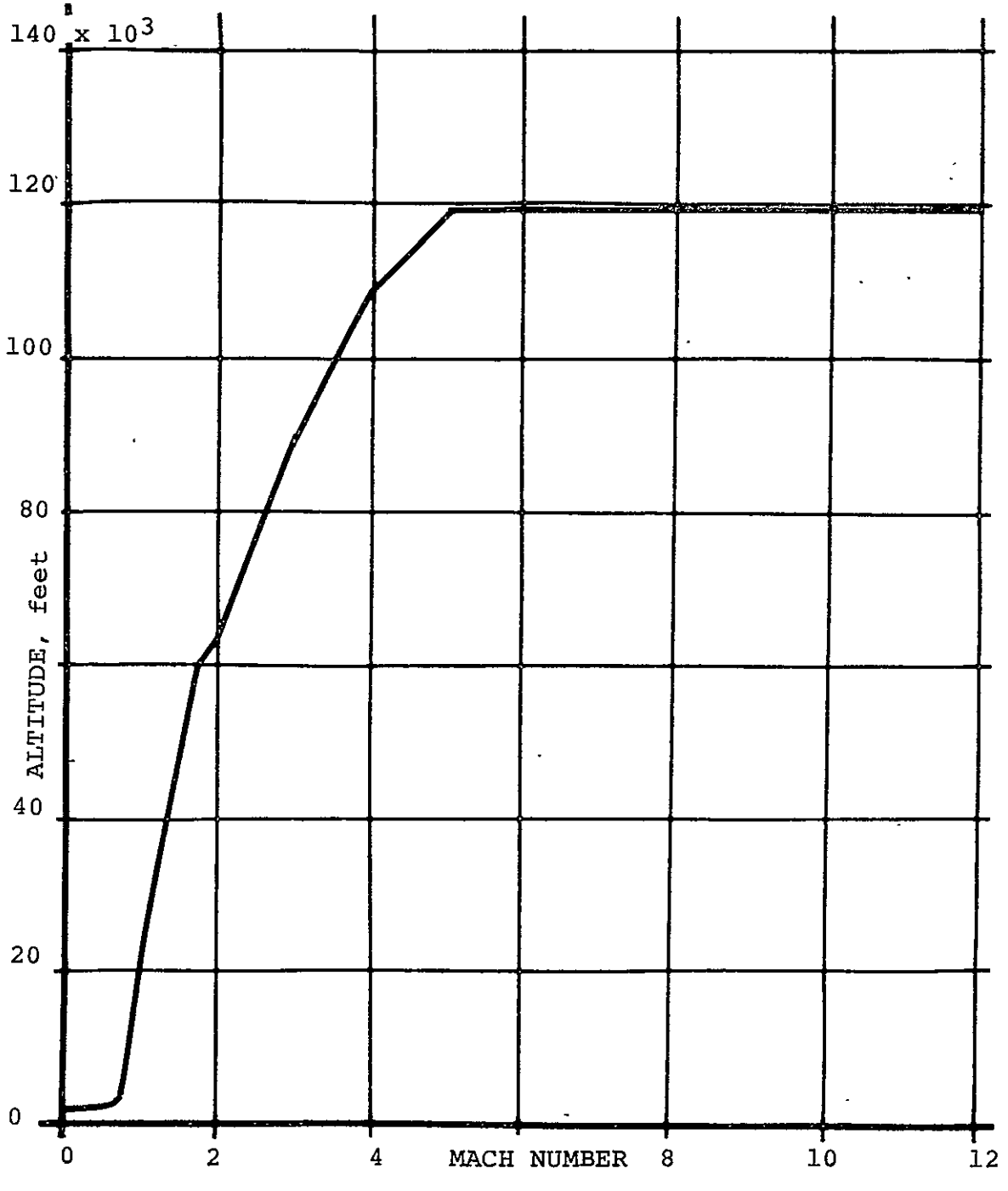

Figure 2.— Parametrically Determined HRA Minimum Time-to-Climb Path

Propulsive Characteristics

The proposed HRA propulsive system is a throttlable rocket engine. Engine characteristics at full throttle are

$$T_{vacuum} = 230{,}000 \text{ lbs.}$$

$$I_{sp_{vacuum}} = 431 \text{ secs.}$$

$$\text{Exit Area} = 18.408 \text{ ft.}^2$$

The data provides a mass flow rate of 16.586 slugs/second and an effective sea level I_{sp} of 358 secs.

Specific impulse attainable is a function of throttle setting; the variation of I_{sp} with throttle setting is presented in Figure 3.

Thrust is always aligned along the vehicle body axis.

Aerodynamic Characteristics

Vehicle aerodynamic coefficients are assumed to be functions of Mach number and angle-of-attack according to the relationships,

$$C_L(M,\alpha) = C_{L_1}(M) \cdot \sin\alpha + C_{L_2}(M) \cdot \sin\alpha \,|\sin\alpha|$$

$$C_D(M,\alpha) = C_{D_o}(M) + K(M) \cdot C_L(M,\alpha) \cdot \sin\alpha \cdot \tan\alpha$$

Values of C_{L_1}, C_{L_2}, and C_{D_o} are tabulated below.

TABLE I.—HYPERSONIC RESEARCH AIRCRAFT AERODYNAMICS

M	CLA1	CLA2	C_{D_o}
0.1	0.894	0.0	.008842
0.5	0.907	0.0	.006889
0.8	0.938	0.0	.006314
1.2	1.057	0.143	.051977
1.5	1.023	0.241	.038967
2.0	0.976	0.373	.029106
3.5	0.853	0.722	.018578
6.0	0.575	1.259	.013054
9.0	0.336	1.603	.010085
12.0	0.219	1.809	.008837

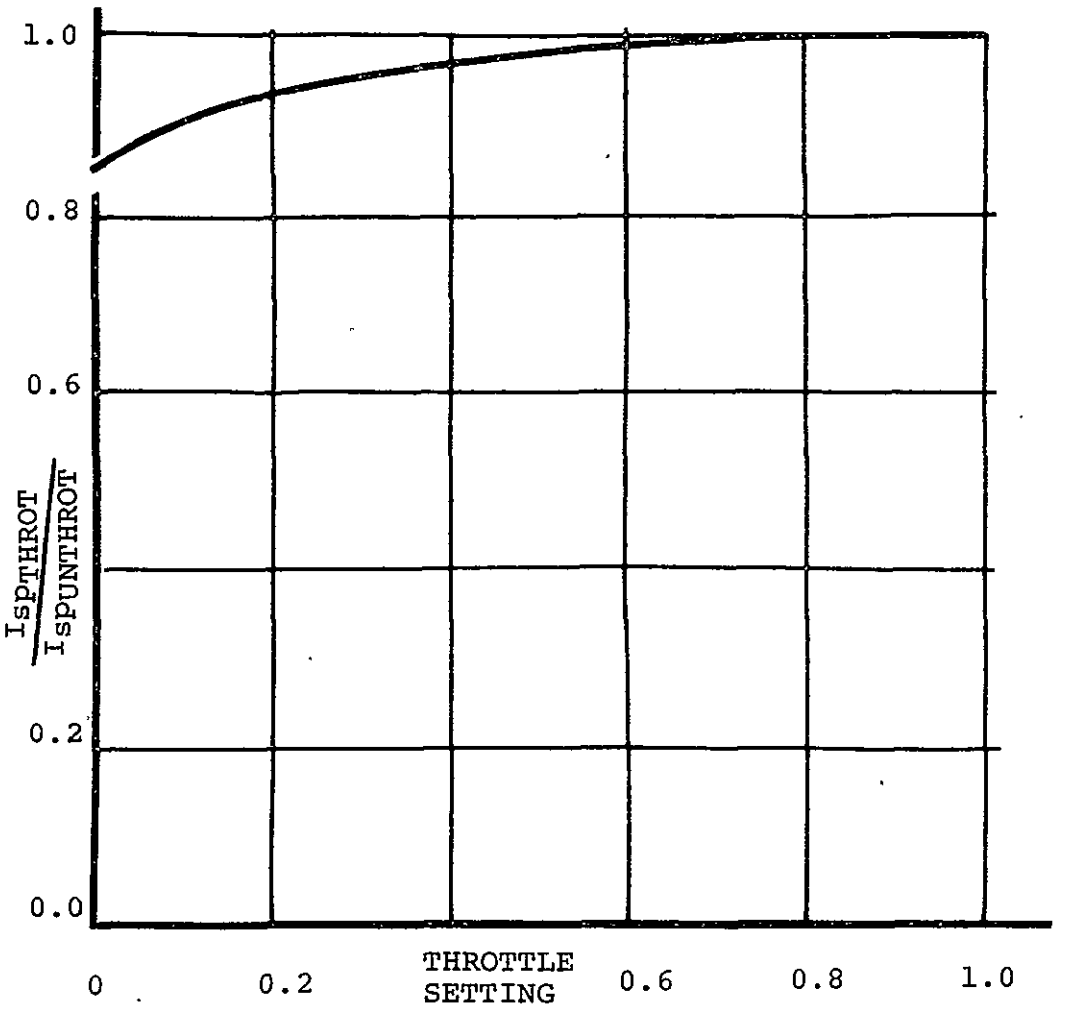

Figure 3.— Variation of I_{sp} with Throttle Setting (HRA)

The factor K is given by

$$K(M) = 0.25\ (1.0 + M); \quad M < 3.0$$

$$= 1.0 \quad ; \quad M \geq 3.0$$

Initial Conditions and Vehicle Parameters

Vehicle conditions at lift-off are

Velocity = 462.17 ft./sec.; 273.8 knots

Altitude = 2300 feet (Take-off at Edwards AFB)

Flight Path Angle = 0.0

Angle-of-Attack = 10.5°

Mass = 4458 slugs

Full Throttle Minimum Time-to-Climb — Terminal Altitude and Velocity Constrained

The minimum time-to-climb path at full throttle was computed by the steepest-descent procedure starting from the two different nominal control histories sketched below.

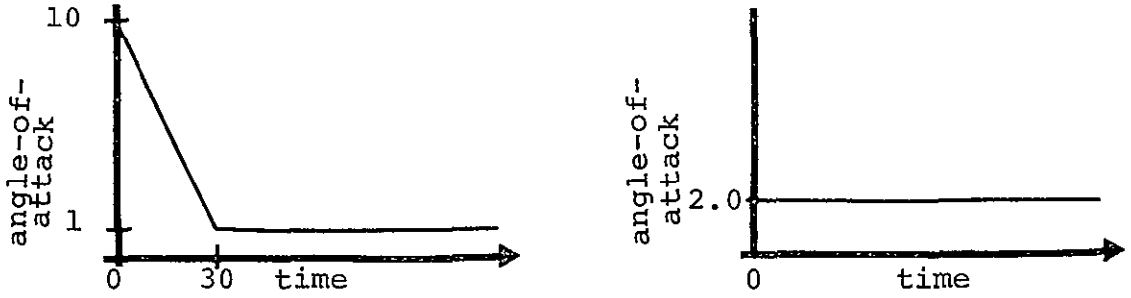

The trajectory optimization calculations may be formally symbolized as follows. (The nomenclature of Reference 1 is employed).

$$\phi = t; \quad \psi = h,V; \quad \alpha = \alpha(t)$$

Desired constraint values are

$$h = 119300 \text{ ft. and } V = 12456 \text{ ft./sec.}$$

The velocity constraint was employed as trajectory cut-off function, Ω, in both solutions. Both solutions converged to essentially the same optimal flight path. Nominal paths and final paths attained are presented in Figure 4. The two final paths are indistinguishable from each other at this scale despite selection of widely differing nominal paths. This demonstrates with some

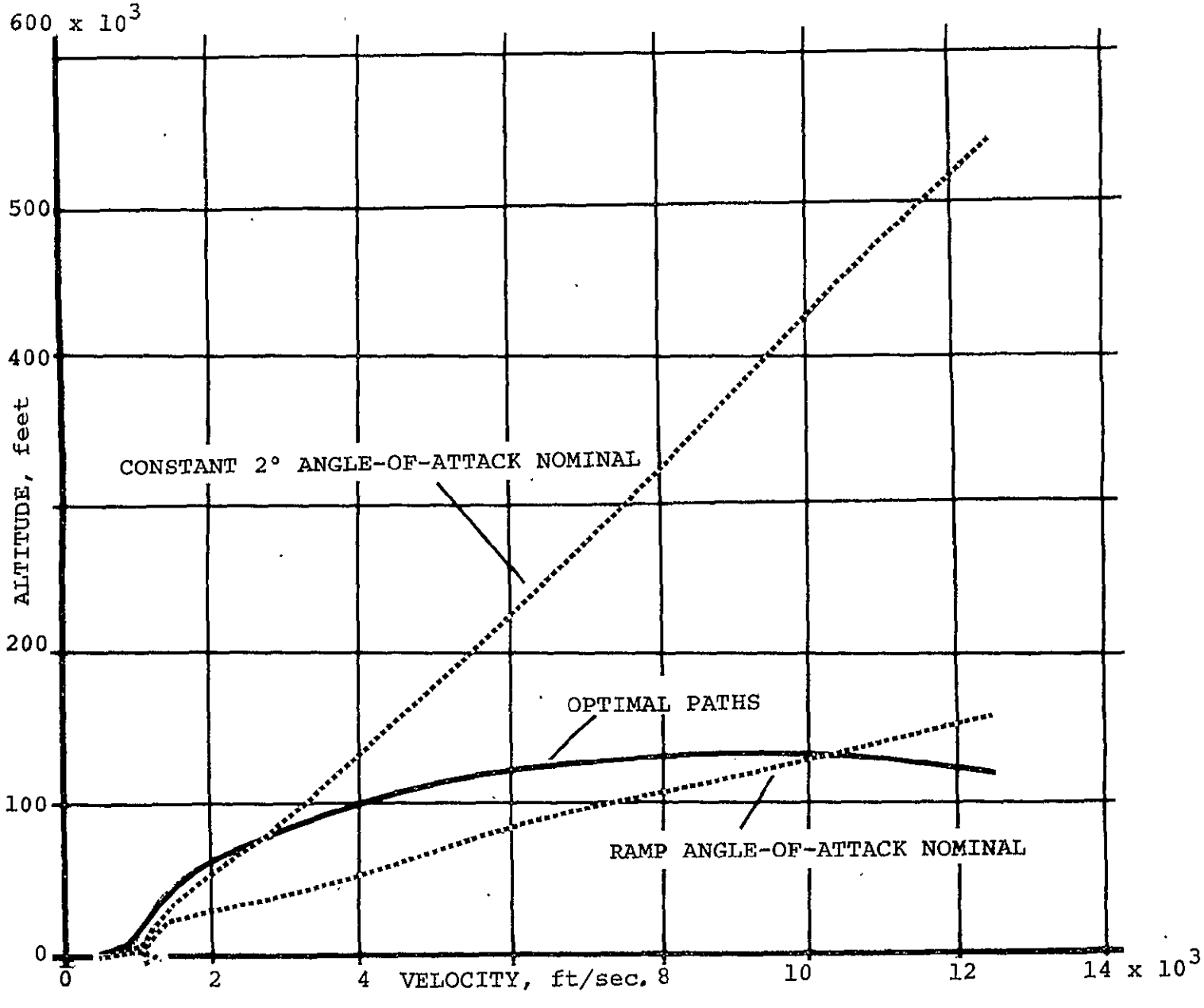

Figure 4.—Nominal and Optimal HRA Paths Full Throttle Minimum Time-to-Climb Constrained Terminal Height and Velocity

degree of certainty the optimality of the final path. The final trajectories are presented to larger scale to allow closer comparison between the two results in Figure 5. It can be seen that the slight discrepancy between the two solutions is due to attainment of slightly different terminal altitude. A final altitude constraint tolerance of ±1000 feet had been permitted in the study. Final constraint values are within this tolerance. The tolerance apparently does not result in significant performance variation. It may be noted that the terminal constraints are achieved in a diving condition. Minimum time-to-climb is 182.8 seconds in both solutions, corresponding to a mass of 1426 slugs, approximately 32 per cent of the mass at lift-off. Transverse acceleration in the pull-up at low velocity is less than 2g. Axial accelerations increase monotonically with time since full throttle is maintained throughout the flight. Final axial acceleration is approximately 4.5g.

Convergence to the optimal flight path is shown in Figures 6 and 7. In both cases the second-order step-size criteria contained in the program of References 1 and 2 automatically determines a regular sequence of perturbations leading to the optimal path. It can be seen from Figure 6, where convergence from the constant 2^{o} angle-of-attack nominal is presented, that the initially large altitude constraint error is decreased monotonically with each iteration cycle. In Figure 7, the convergence behavior is somewhat different. The relatively small initial altitude constraint error is permitted to increase in order to provide greater initial performance improvements. After four iterations, the convergence logic reverts to more regular decisions leading to further, almost monotonic, convergence of both performance and constraint functions. In both calculations velocity was employed as cut-off function. This terminal constraint is thus satisfied on all trajectories. Selected state component histories are presented in Figure 8.

Full Throttle Minimum Time-to-Climb With Additional Terminal Level Flight Constraint

The minimum time-to-climb optimal ascent path obtained in the preceding section has two unanticipated and possibly undesirable features. These are the negative terminal flight path angle (γ=-4.4°) and the altitude overshoot prior to attainment of flight path terminal state. An investigation of the performance penalties associated with these two trajectory features was undertaken. In this section an optimal ascent was obtained with a terminal level flight constraint (γ=0.0) imposed. In the following section an optimal ascent with both the terminal level flight constraint and an in-flight constraint preventing instantaneous altitude from significantly exceeding terminal altitude ($h(t) \leq 120000$ ft)

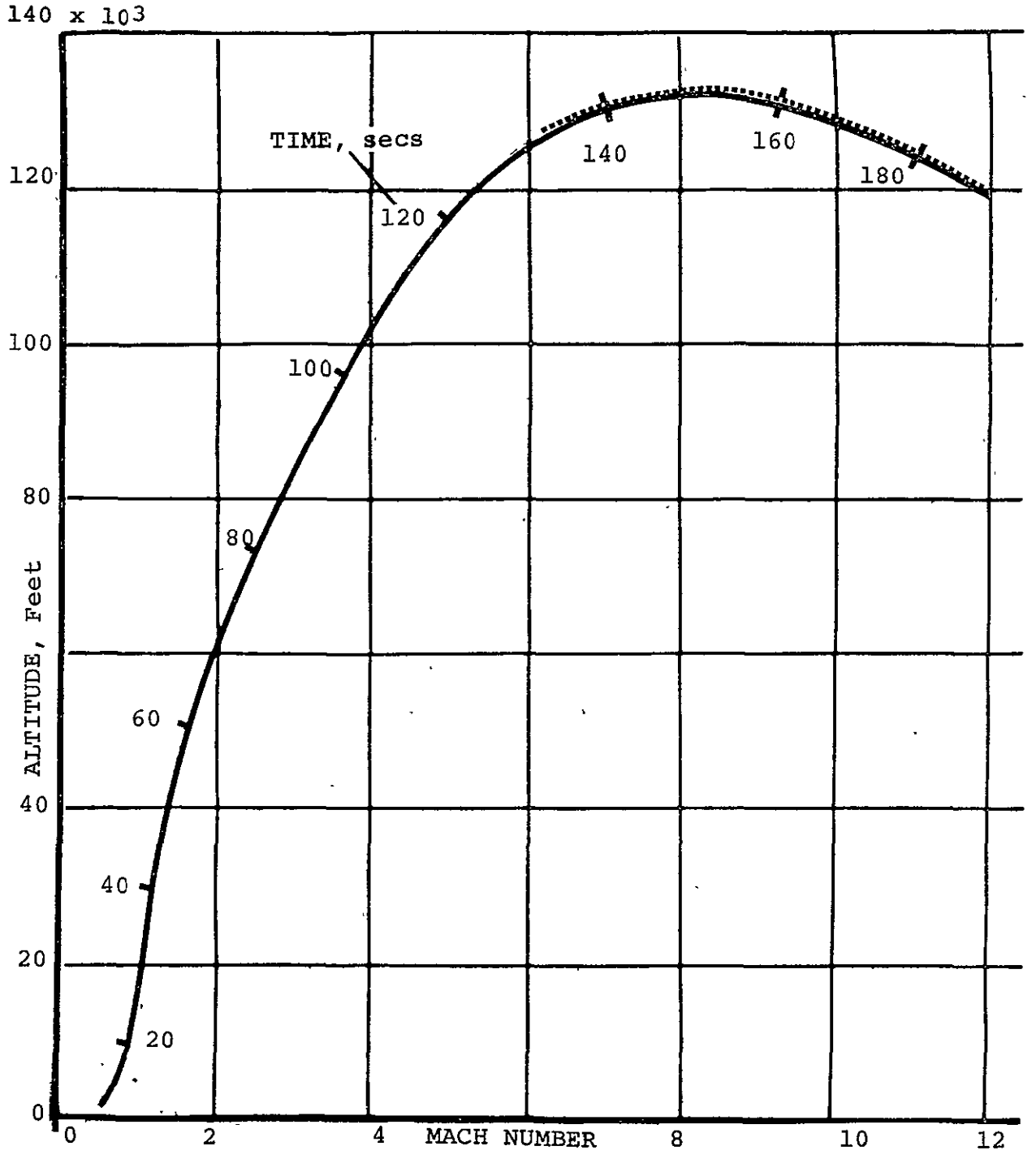

FIGURE 5.—DETAILED COMPARISON OF OPTIMAL HRA ASCENT PATHS OBTAINED FROM TWO NOMINAL STARTING PATHS

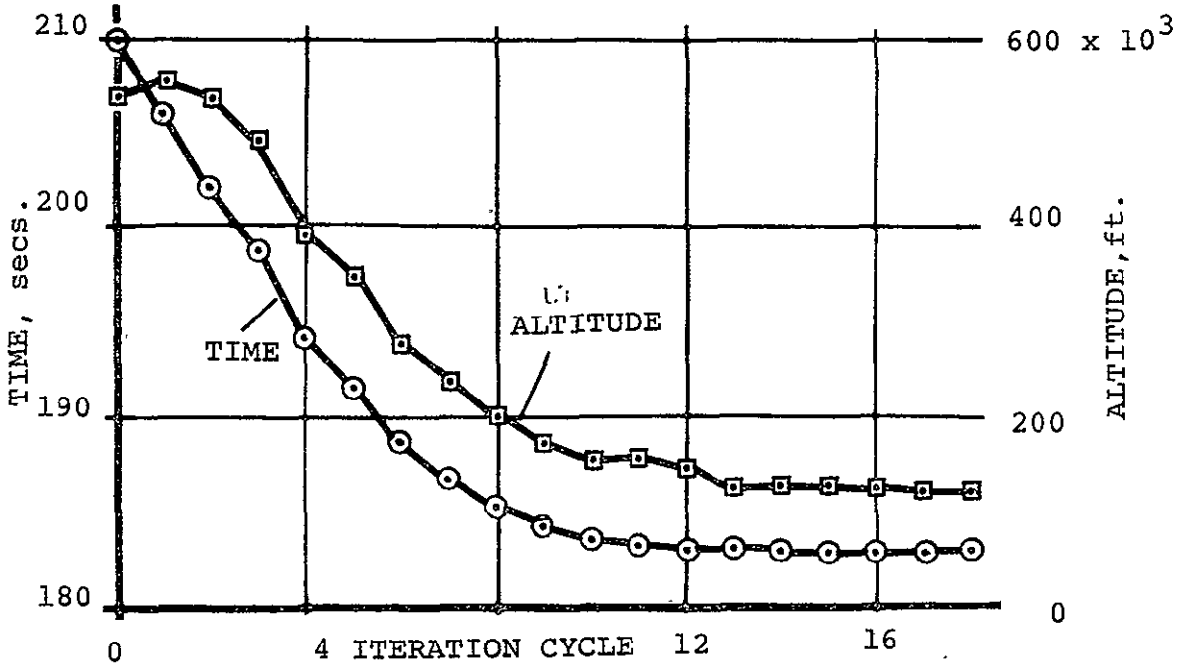

Figure 6.— Convergence Plot from Constant α Nominal, Altitude and Velocity Constrained

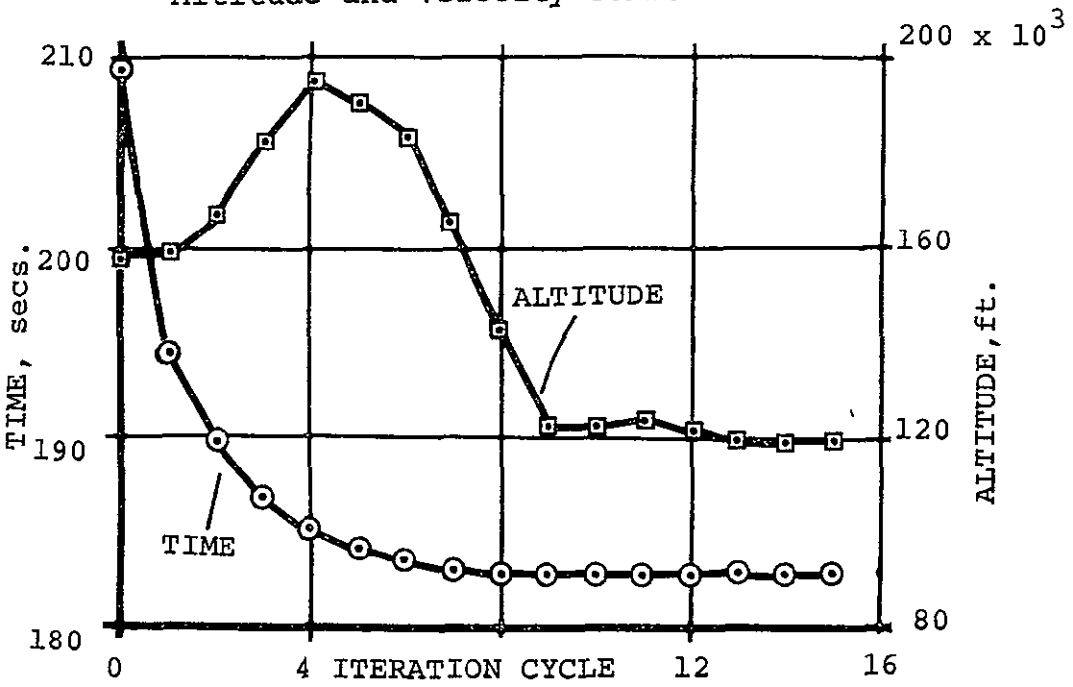

Figure 7.—HRA Trajectory Convergence Plots from Ramp α Nominal, Altitude and Velocity Constrained

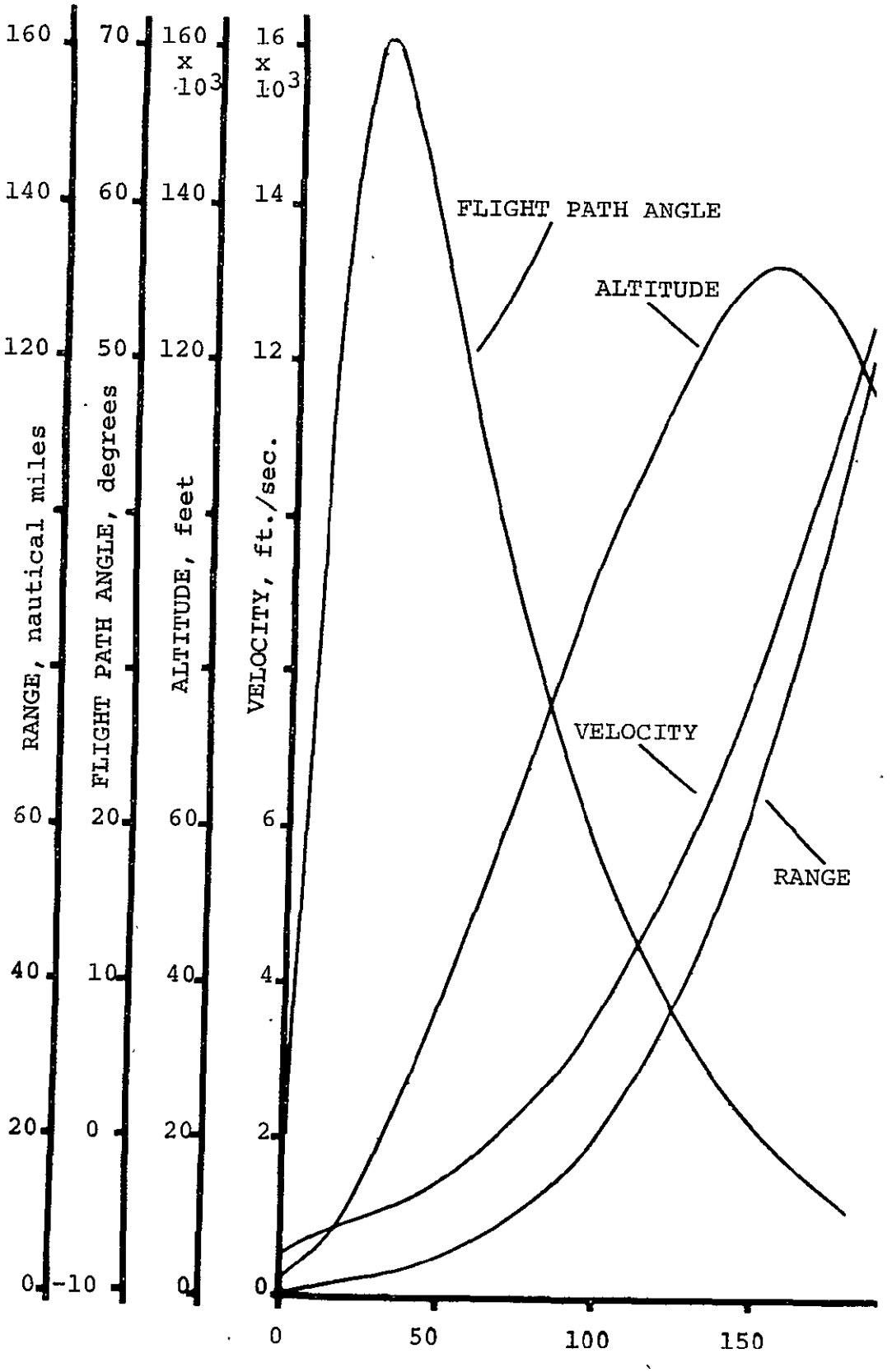

Figure 8.—State Component Histories, HRA Minimum Time-to-Climb

is obtained. With terminal altitude velocity and flight path angle constrained, the solution can be symbolically described by

$$\phi = t; \quad \psi = h,V,\gamma; \quad \alpha = \alpha(t)$$

The trajectory attained with this problem statement is presented in Figure 9. The figure also includes the constrained altitude and velocity solution described in the previous section for comparison purposes. Velocity was again employed as the cut-off function.

The addition of a level flight constraint causes a considerable reduction in altitude overshoot. Minimum time-to-climb becomes 183.5 seconds, a slight increase over the time of 182.8 seconds attained without the flight path angle constraint. Terminal mass of 1414 slugs is approximately 1 per cent less than the γ-free solution. It is apparent from Figure 9 that the optimal γ-free and γ-constrained trajectories are similar in character. The initial pull-up in the two optimal trajectories are indistinguishable from each other. The trajectories begin to show measurable differences at about a Mach number of 3. At this point, the vehicle has achieved an altitude in excess of 80,000 feet. Trajectory apogee in the γ-constrained case is 125,000 feet, achieved approximately two and one-half minutes after lift-off. This compares with an apogee of 133,000 feet in the γ-free trajectory. In both cases apogee is achieved at approximately Mach 9,and an accelerating descent to terminal state immediately follows.

The relatively smooth trajectory perturbation utilized to achieve the additional constraint and associated small change in performance is typical of the optimal performance technique. Intuition might have suggested that the additional constraint should be met by following the γ-free path to apogee then performing a gradual pull-out to achieve level flight at the desired velocity and altitude. Alternatively, one might anticipate that a small change in flight path angle at lower speed might propagate along the trajectory and provide an efficient means for accomplishing terminal level flight, analogous to the launch vehicle "kick-angle." Apparently, the optimal way to achieve level flight is a compromise between these two intuitional approaches. It is possible, of course, that the performance difference between the various methods of achieving level flight is small. This possibility was not investigated during the present study.

A note on convergence is in order. The optimal γ-constrained solution was sought from both the ramp and the constant angle-of-attack nominal controls employed in the previous section. From the ramp history convergence to the optimal path was rapid and well-behaved. From the constant angle-of-attack nominal control history, on the other hand, convergence was initially quite slow with the flight path

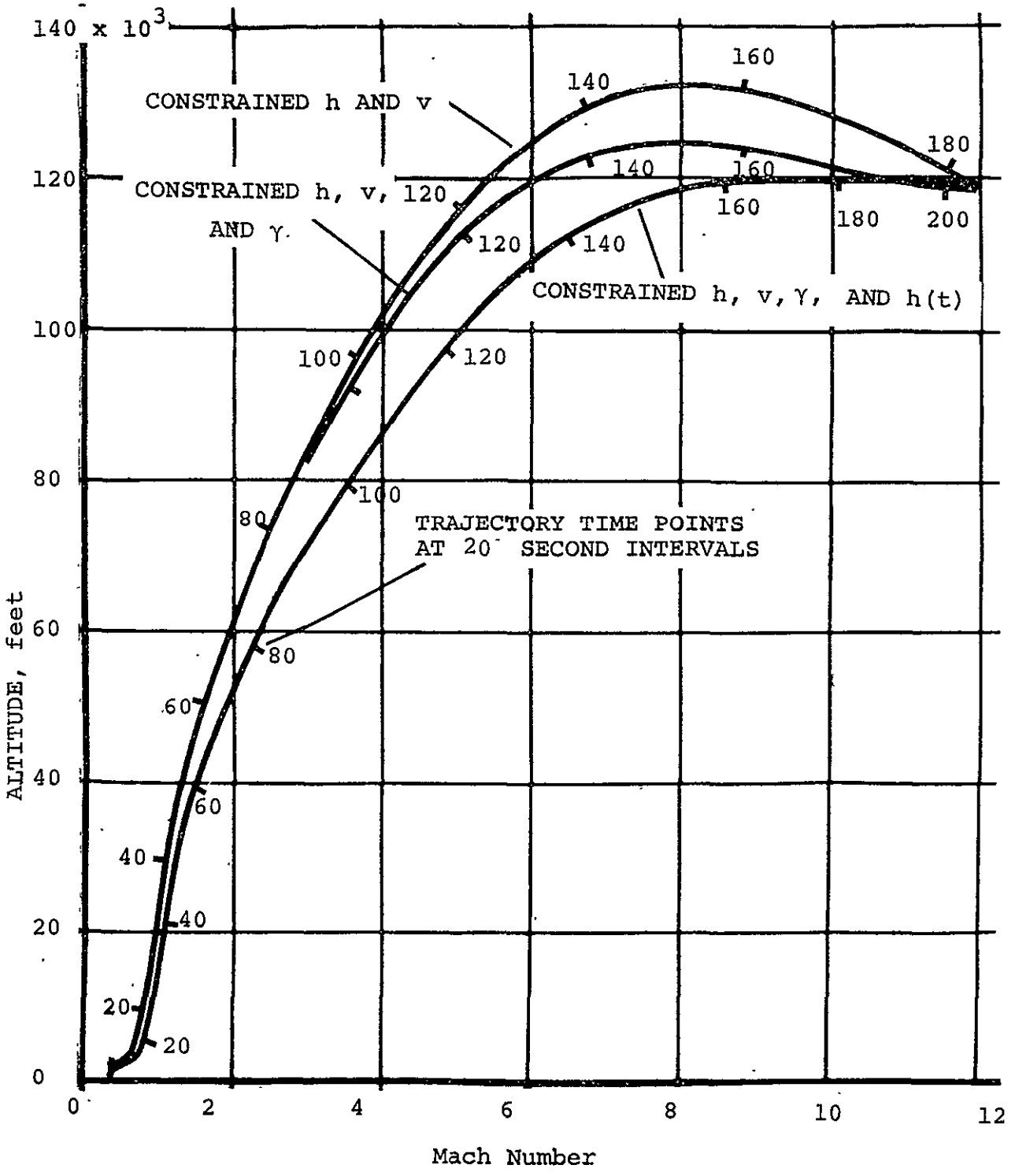

Figure 9.—Comparison of Optimal HRA Constrained Ascent Paths

angle constraint being ignored until the seventeenth iteration. At this point performance and both constraints began to simultaneously improve. Convergence from both nominals is tabulated in Table II. The solution being obtained from the constant angle-of-attack nominal was abandoned at 18 iteration angles in view of the rapidly convergent solution obtained from the constant angle-of-attack nominal.

HRA Full Throttle Minimum Time-to-Climb with Additional Terminal Level Flight and In-Flight Attitude Constraint

In view of convergence behavior reported in the previous section, the optimal ascent trajectory subject to additional constraints of terminal level flight and in-flight inequality constraint on maximum altitude was obtained from the ramp angle-of-attack nominal control history. Symbolically, this solution can be expressed as

$$\phi = t; \quad \psi = h, V, \gamma, h(t); \quad \alpha = \alpha(t)$$

The final trajectory is shown on Figure 9, page 14. Convergence behavior is presented in Table III. These results are also presented graphically in Figure 10. Velocity was used as cut-off function and, hence, is satisfied on all trajectories.

It can be seen that convergence is quite regular but slow. At iteration cycle 16, the weighting matrix was changed from

$$(W(t))^{-1} = 1$$

to

$$(W(t))^{-1} = 300 - t$$

This weighting matrix was selected from visual inspection of the trajectory generated by 16 iterations. It appeared that for this trajectory convergence of the initial part of the trajectory was slow, notably at the higher Mach number at which the initial pull-up occurred. In an attempt to speed convergence of the initial part of the trajectory, the time-varying weighting matrix above was selected. This matrix attempts to force approximately three times greater perturbation at the trajectory initial point then at the final point. It appears questionable that the weighting matrix change produced quicker convergence in light of subsequent behavior recorded on Figure 10.

From cycle 30 onwards the perturbation magnitude selected by the stepsize logic in the program of References 1 and 2 was over-ridden by depressing sense switch 4 on the IBM 7094

TABLE II.—
CONVERGENCE BEHAVIOR FROM TWO NOMINALS WITH THREE TERMINAL CONSTRAINTS

	Solution from Ramp α Nominal			Solution from Constant α Nominal		
Cycle	ϕ	ψ_1(h)	ψ_2(γ)	ϕ	ψ_1(h)	ψ_2(γ)
0	208.85	156217	10.17	209.71	543752	56.51
1	202.38	144061	9.126	211.12	526584	56.47
2	194.29	128788	6.246	212.42	511569	56.53
3	187.50	131944	3.587	213.75	496458	56.58
4	185.91	134010	2.753	215.19	480341	56.61
5	184.73	136441	2.025	216.64	464208	56.62
6	183.74	141314	1.560	217.89	450331	56.58
7	183.67	133755	1.314	219.50	433971	56.75
8	183.42	129956	.7852	221.06	417142	56.67
9	183.08	134298	.4837	222.69	399522	56.50
10	183.35	126190	.5021	224.37	381912	56.37
11	183.09	130540	.3026	225.95	365157	56.18
12	183.31	125487	.2995	227.19	353729	56.41
13	183.37	123794	.1599	229.15	328226	54.71
14	183.20	126040	.0815	234.71	295029	59.35
15	183.37	122210	.0913	238.45	267998	61.31
16	183.36	122470	.0772	241.46	246275	62.98
17	183.62	118744	.2652	240.60	213740	54.35
18	183.58	118643	.1038	235.18	146623	34.66
19	183.57	118658	.0925			
20	183.54	118884	.0398			

NOTE: Velocity employed as cut-off function

TABLE III.—

HRA TRAJECTORY CONVERGENCE FULL THROTTLE MINIMUM TIME ASCENT WITH FOUR CONSTRAINTS

Cycle	ϕ	ψ_1 (h)	ψ_2 (γ)	ψ_3 ($\int \Delta h.dt$)
0	208.85	156217.	10.172	316930.
1	202.98	145205.	8.914	174737.
2	211.68	127752.	8.593	172489.
3	208.19	127038.	9.907	122641.
4	208.79	126374.	8.949	10648.
5	211.46	124862.	8.420	6908.
6	213.60	121538.	7.244	719.
7	213.63	122337.	6.763	1905.
8	208.42	117270.	4.973	0.
9	204.29	115807.	3.625	0.
10	193.73	114401.	1.804	0.
11	190.28	121026.	1.378	1794.
12	189.74	121208.	1.316	2559.
13	189.87	121245.	1.294	2993.
14	190.10	121283.	1.255	3431.
15	190.27	121232.	1.207	3382.
16	190.42	121122.	1.125	3207.
17	190.54	121021.	1.062	2927.
18	190.77	120935.	.918	3415.
19	190.44	120821.	.731	4311.
20	190.14	120488.	.420	5609.
21	189.70	119922.	.036	6525.
22	189.27	119530.	.032	1503.
23	189.02	119535.	.001	2087.
24	188.63	119341.	- .013	817.
25	188.54	119458.	- .002	1190.
26	188.46	119567.	- .005	2338.
27	188.35	119249.	- .005	164.
28	188.32	119314	.001	149.
29	188.28	119249.	- .001	4.02
30	187.36	122836.	.0160	71281.
31	187.24	119184.	.081	3346.
32	186.25	121750.	.082	45704.
33	185.94	121910.	.049	55731.

NOTE: Velocity employed as cut-off function

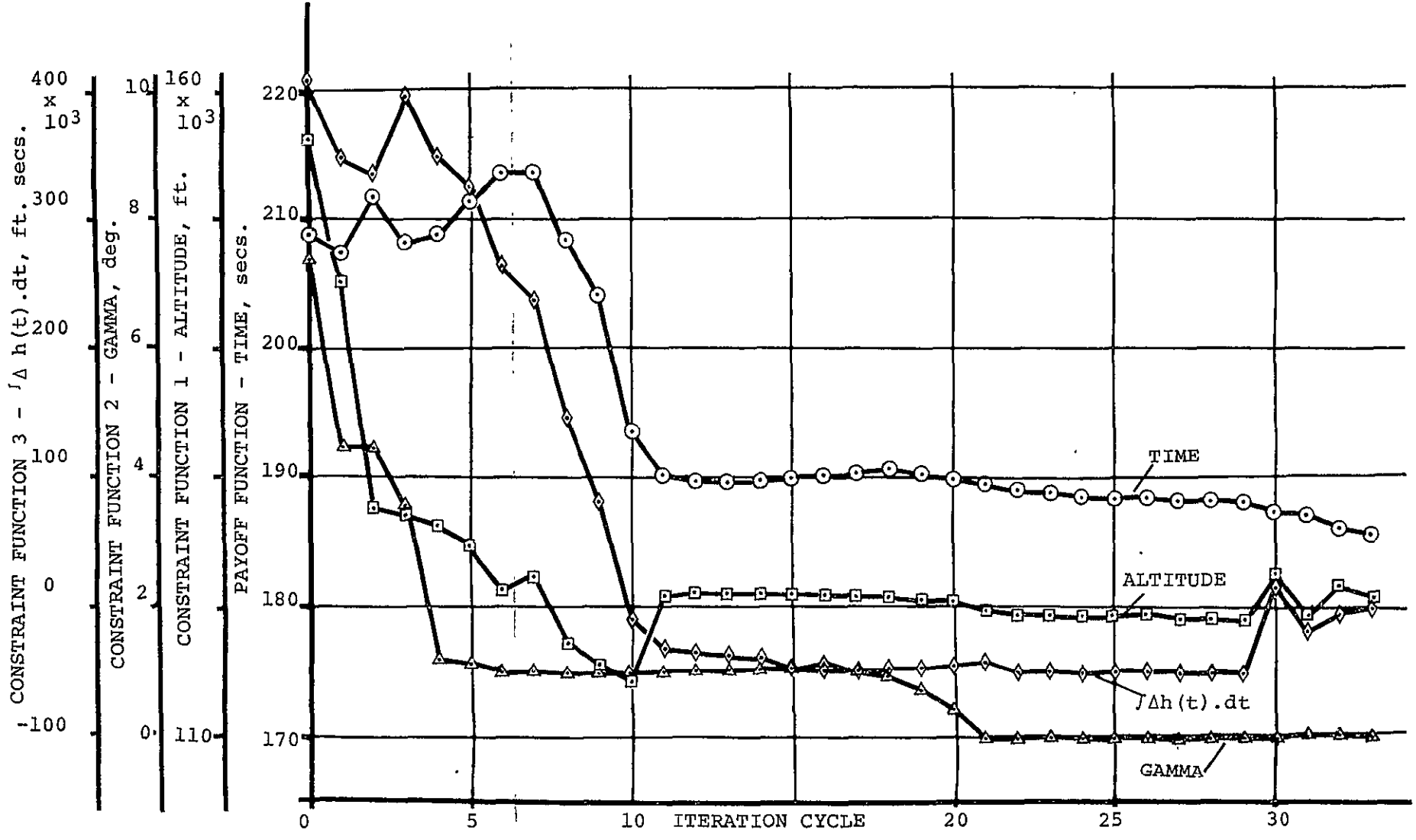

Figure 10.—HRA Convergence Plot Three Constraints

console. (This action also causes detailed trajectory printouts to be obtained). At this point the performance which had previously appeared to practically converge began to improve at the expense of the two altitude constraints.

Since it appears from previous results that terminal altitude does not exert a powerful influence on performance in the range of altitudes involved, performance variations in the last cycles were plotted against the altitude inequality constraint violation. In this way it was hoped that the apparent performance improvement in these cycles could realistically be assessed. The result is shown in Figure 11. It can be seen that iteration cycles 31, 32, and 33 fall on a smooth curve. Further, the inequality violation present on the previously obtained terminal altitude velocity and flight path angle constrained solution was also computed. This additional point also falls on the curve presented in Figure 11. The inference is that the performance gains in the last cycles of Figure 10 are due to constraint violations. Hence, the solution attained at cycle 31 which has negligible constraint violation is taken as the optimal result. Figure 11 thus presents an approximate variation of minimum time-to-climb with altitude overshoot.

This solution is the one presented in Figure 9. It can be seen that the altitude inequality constraint has effectively introduced a constant altitude sub-arc along the altitude inequality. The boundary is acquired in a smooth manner at approximately Mach 8.5. The vehicle then accelerates at constant altitude to the desired terminal state. Below Mach 8.5 the trajectory shows a marked departure from the previously obtained, less constrained paths. The transonic pull-up persists, however.

It appears from Figure 9, that the optimal way to satisfy the altitude inequality is by a transonic "kick-angle" maneuver which achieves level flight on the altitude inequality constraint boundary followed by the constrained sub-arc acceleration.

Performance loss associated with satisfaction of the inequality constraint is quite large. The minimum time ascent now requires 187.3 seconds. This is 4.5 seconds longer than the solution obtained when only terminal altitude and velocity are constrained. The mass reduction corresponding to this increased flight time is 74 slugs or approximately 2350 lbs.wt. This five per cent loss in <u>total</u> terminal mass is a high performance penalty for removal of the altitude overshoot. This is particularly so if the performance loss is compared with usable terminal payload. Hence, it appears that HRA ascent paths will be typified by altitude overshoots of the type shown in Figure 9, at least for thrust-to-weight ratios approaching that of the vehicle under study.

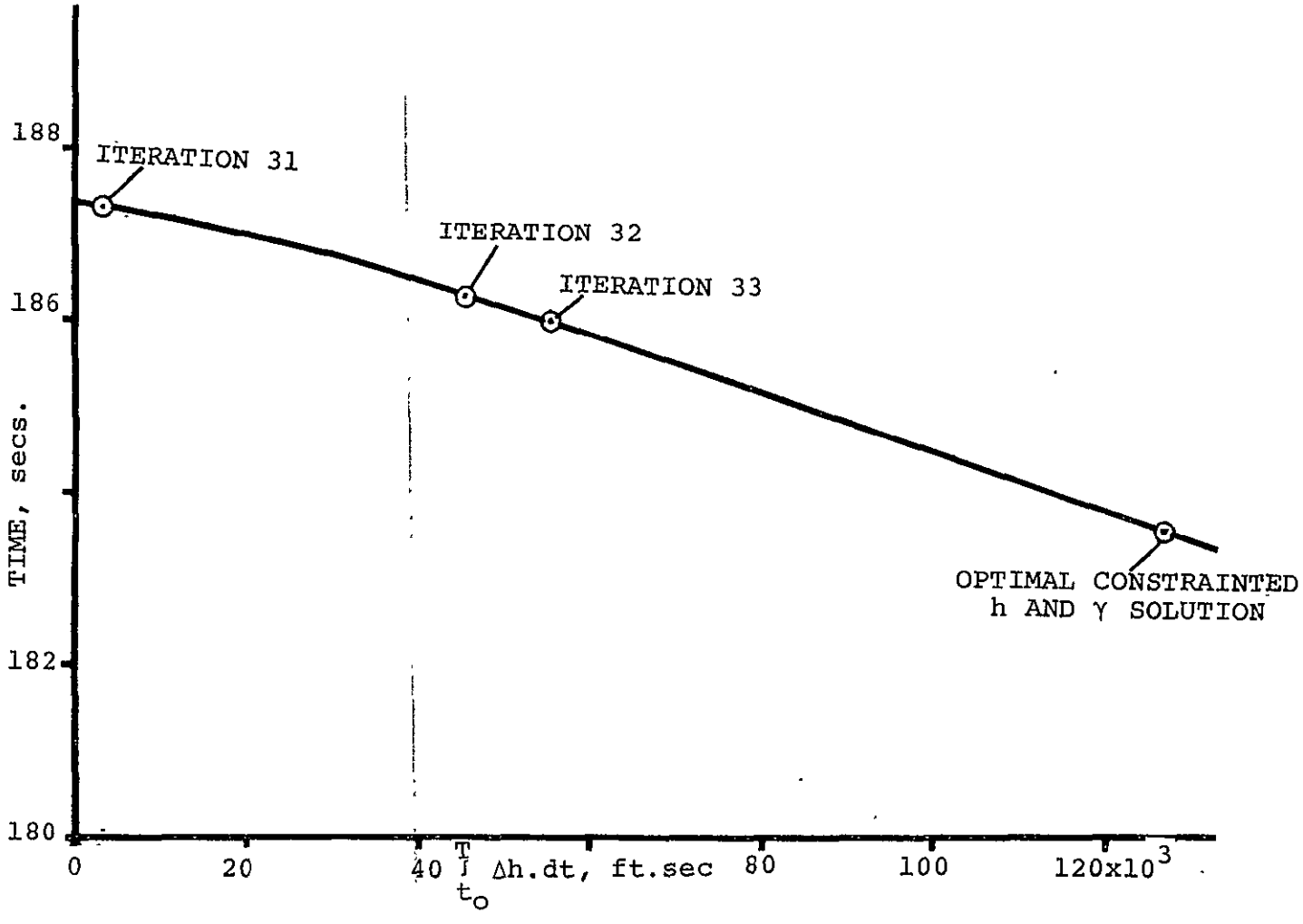

Figure 11.— Variation of HRA Time to Climb with Allowable Altitude Overshoot

Throttle Free Maximum Payload Ascent
Terminal Velocity and Altitude Constrained

Payload was maximized subject to terminal constraints on velocity (12456 ft./sec., Mach 12) and altitude (119300 feet). Two continuous control variables, angle-of-attack and throttle setting,were employed. Use of throttle setting as a control variable requires replacement of the minimum time performance criteria employed previously by a maximum mass criteria. Realistic thrust limits are imposed by means of an inequality constraint restricting throttle to be less than or equal to 1.0 (the value corresponding to maximum thrust). Symbolically these trajectories can be described as

$$\phi = -M; \quad \psi = h,V,N(t); \quad \alpha = \alpha(t), N(t)$$

As in previous examples, velocity is employed as cut-off function and, hence, is satisfied on all trajectories. The ramp angle-of-attack history previously employed and full throttle were used in nominal trajectory generation.

Two solutions were obtained. Both used the same nominal trajectory as a starting point; however, the weighting matrix employed in each calculation was varied. Convergence of the first solution, employing a unit weighting matrix,is presented in Figure 12 . Convergence of the second solution, which employed

$$[W] = \begin{bmatrix} 1. & 0. \\ 0. & 100. \end{bmatrix}$$

is shown in Figure 13.

This weighting matrix was selected on the basis of the integral of the absolute values of control impulse response functions along the final trajectory of the first solution. These integrals were 14464 for angle-of-attack control and 2208 for throttle control. Since use of the unit weighting matrix might have tended to inhibit development of the optimal throttle history, the second solution which accentuates throttle perturbations at the possible expense of angle-of-attack perturbations was obtained.

It can be seen that both solutions converge in a generally similar fashion. As might be anticipated, the maximum value of throttle inequality violation is some two orders of magnitude greater when the throttle accentuating weighting matrix is employed. However, in both cases, convergence is well behaved. Final mass values obtained in the two calculations are 1427 slugs and 1428 slugs for the unit weighting matrix and throttle accentuating weighting matrix solutions, respectively. These figures and the reasonable satisfaction of constraint values

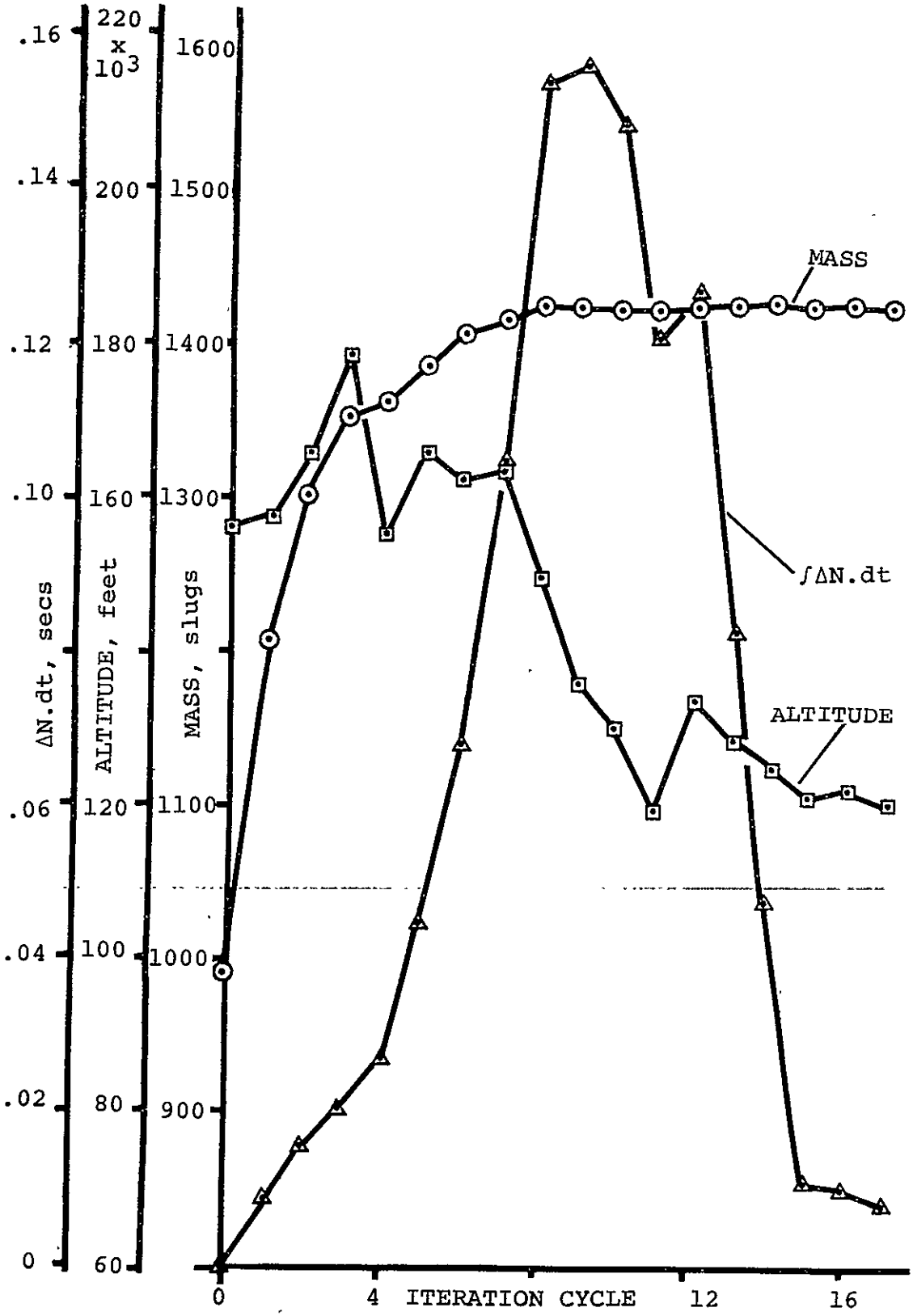

Figure12.— HRA Maximum Terminal Mass Ascent Convergence Plot, [W] = [I]

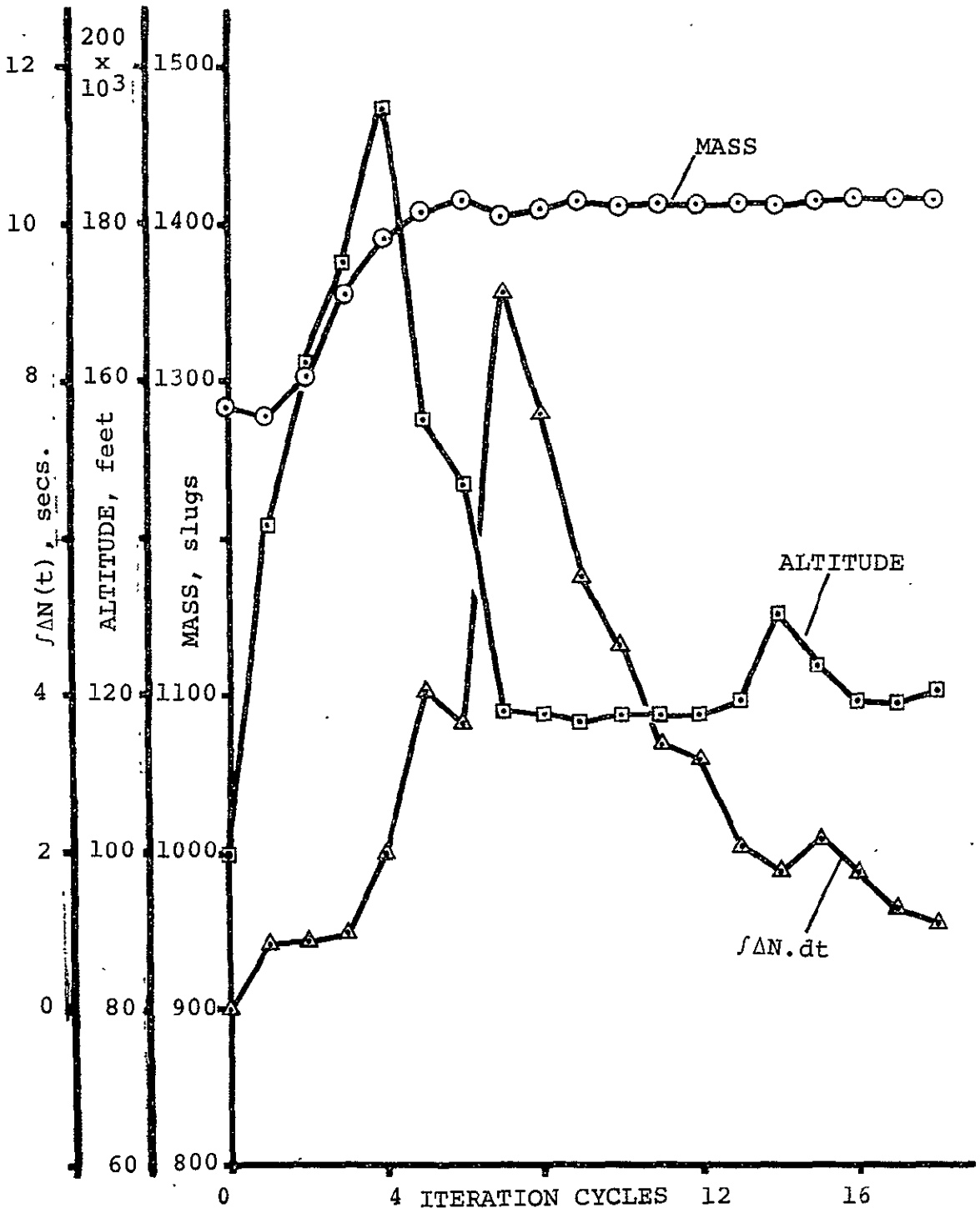

Figure 13.—HRA Maximum Terminal Mass Ascent-Convergence Plot Throttle Accentuating Weighting Matrix

confirm the optimality of solution. Freeing throttle permits a very slight two-slug performance gain over the throttle fixed case.

Time to ascend is approximately 209 seconds or 26 seconds longer than the minimum time (maximum terminal mass) full throttle ascent. This time increase is primarily due to engine throttling. A description of throttle history is deferred until the next section where an additional inequality constraint is placed on the vehicle axial acceleration. The final trajectory attained is presented in Figure 14 together with the full throttle minimum time-to-climb solution and subsequently described acceleration limited solutions for comparison purposes.

Throttle Free, Maximum Mass Ascent with Terminal Altitude And Velocity Constraints and In-Flight Acceleration Limit

An acceleration in-flight inequality constraint was added to the constraints imposed on the solution in the immediately preceding section. The inequality was placed on the axial component of acceleration measured in body axis coordinates. For the HRA this corresponds to the line-of-thrust acceleration. This component of acceleration was limited to be less than or equal to 3g. Velocity was employed as the cut-off function. Symbolically, the problem can be stated

$$\phi = -M; \quad \psi = h, V, N(t), A_x(t); \quad \alpha = \alpha(t), N(t)$$

Terminal flight path angle is left free and an altitude overshoot is permissible. The optimal trajectory is depicted in Figure 14. It can be seen that the solution lies everywhere above both throttle free and throttle fixed terminal altitude and velocity constrained solutions reported earlier. Selected state-component histories are presented in Figure 15. Nominal and optimal control histories for this solution are contained in Figure 16. A convergence plot is presented in Figure 17.

It can be seen from Figure 17 that convergence is quite regular. Performance and acceleration constraint convergence, in particular, are very well behaved. Behavior of the throttle inequality is typical of a non-linear-constraint which is satisfied on the nominal path. In order to maintain reasonably sized gains in the performance and remaining constraints, the throttle inequality constraint progressively deteriorates. At cycle 20 the inequality constraint violation growth is terminated by the program internal perturbation step-size logic. From this point onwards, the constraint shows monotonic improvement as the violation is progressively eliminated.

The problem is essentially solved in 28 iteration cycles. Somewhat slower convergence than was obtained in the earlier, less restrained solutions. However, in the problem stated, despite the use of only five basic state equations for point mass motion

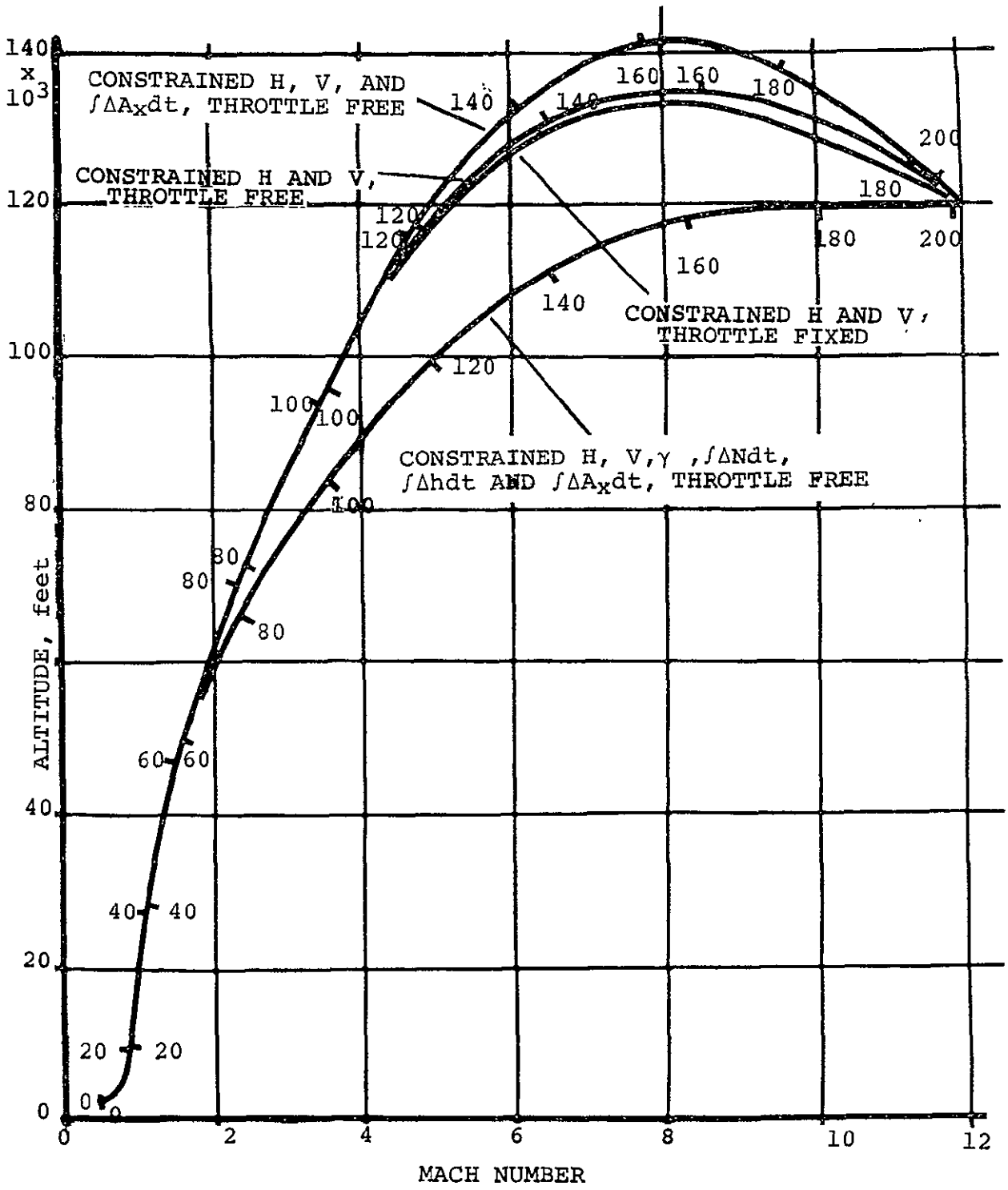

Figure 14.—Comparison of Throttled Optimal HRA Ascent Paths

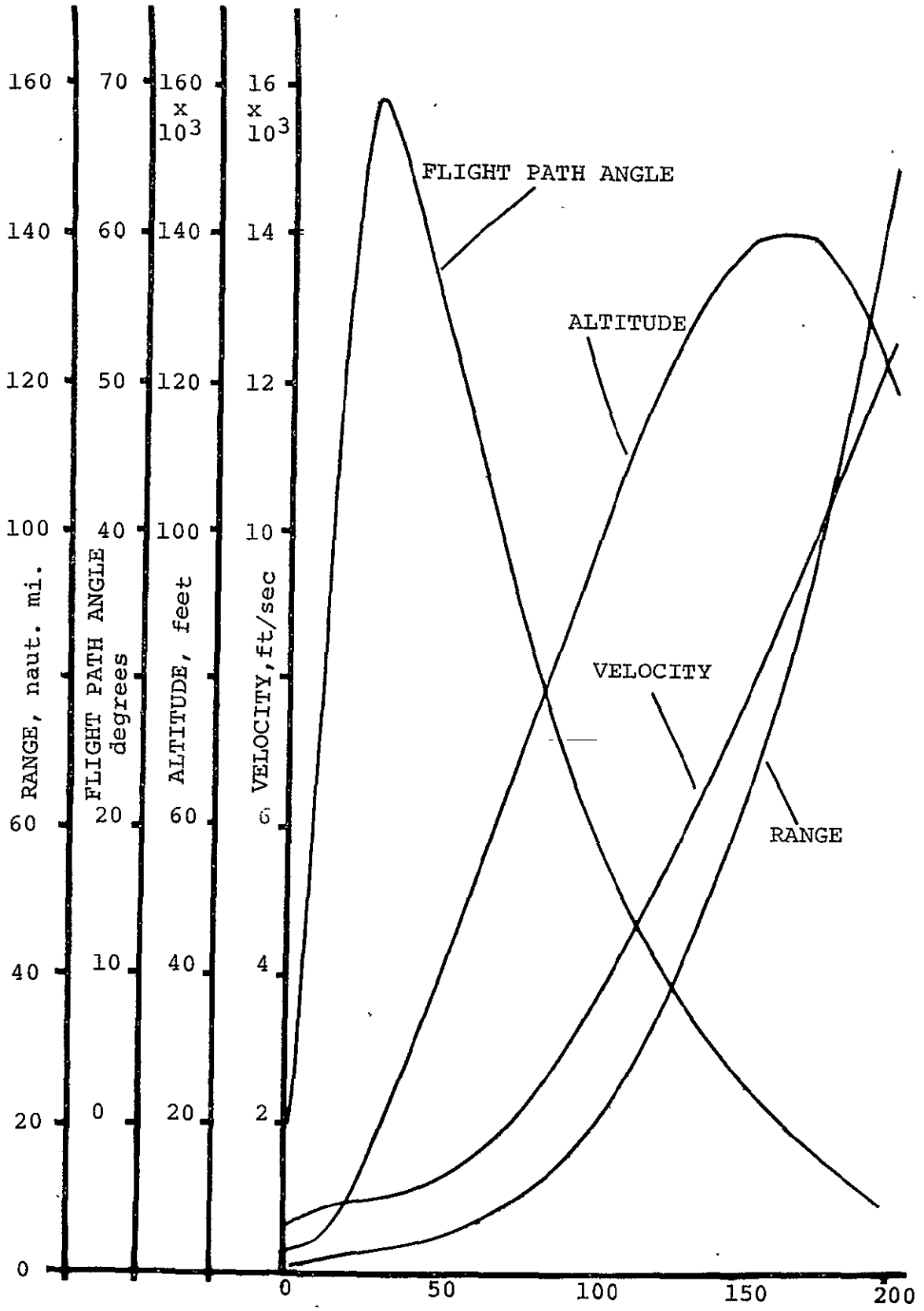

Figure 15.—State Component Histories, HRA Throttle Free Maximum Mass Ascent. Terminal Altitude, Velocity, $\int \Delta N dt$ and $\int \Delta A_x dt$ Constrained

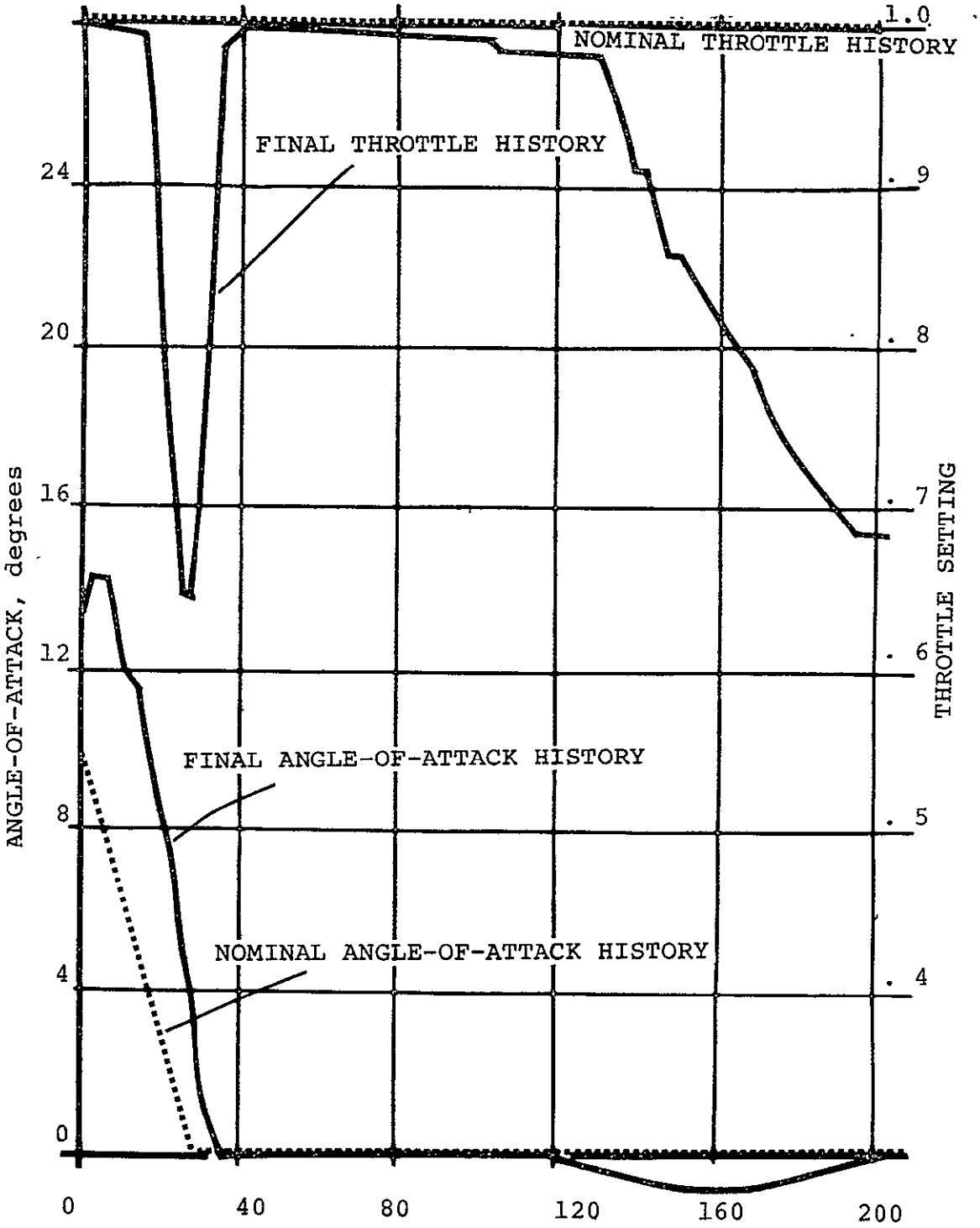

Figure 16.—Nominal and Final Control Histories HRA Throttle Free Maximum Mass Ascent, Terminal Altitude, Velocity, $\int \Delta N dt$, and $\int \Delta A_x dt$ Constrained

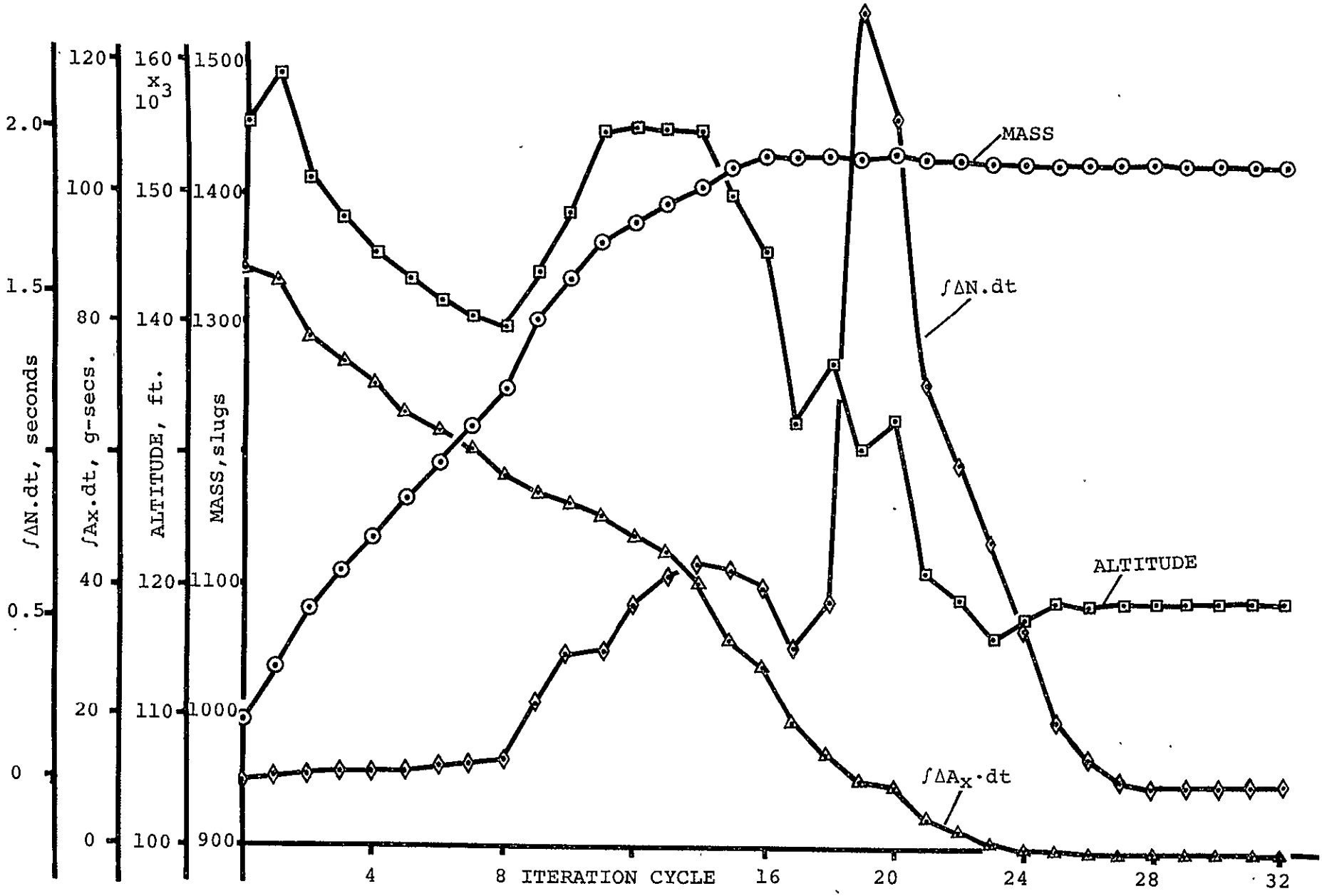

Figure 17.—Convergence Plot HRA Maximum Mass Ascent to H=119300, V=12456, Acceleration Limited

in the equatorial plane, the complete state vector includes seven components. An additional state variable is automatically constructed for each inequality. The problem involves seven state variables, two control variables, four constraints and is therefore fairly complex.

Weighting matrix selection was based on experience with the previous HRA solutions,

$$(W_{11} = 1., \quad W_{22} = 10., \quad W_{12} = W_{21} = 0)$$

The control histories of Figure 16, reveal that most of the ascent occurs at essentially zero lift and almost full throttle. This portion of the flight path is preceded by a pull-up employing an almost linearly decreasing angle-of-attack history. Initially, full throttle is employed in the pull-up. After approximately ten seconds, throttle is progressively decreased until 65 per cent throttle is reached at about thirty seconds from lift-off. Throttle then progressively increases until full throttle is regained 40 seconds from lift-off. At 130 seconds from lift-off the acceleration inequality constraint becomes active, as illustrated in Figure 18. From this point onwards an almost linearly decreasing throttle setting history is employed. It can be seen from Figure 16 that as the vehicle passes through apogee, a small amount of negative lift (maximum of 1^{o}) is imposed in a smoothly varying, almost sinusoidal fashion.

Maximum flight path angle achieved in the ascent is approximately 70^{o} at 30 seconds from lift-off, Figure 15. Maximum altitude is slightly greater than 140,000 feet, almost 10,000 feet higher than the full throttle constrained altitude and velocity solution, Figure 14. Total ground range in the ascent is over 146 nautical miles in 202 seconds flight time. This compares with only 121 nautical miles ground range in 183 seconds flight time for the full throttle altitude and velocity constrained solution. It appears from this result that throttle variation may provide a means for increasing ground range capability of the hypersonic research aircraft; for the terminal mass in the present acceleration limited solutions is 1426 slugs. Hence, the acceleration limit does not impose a significant performance penalty, for this terminal mass equals that obtained at full throttle and is only marginally less than was attained in throttle and acceleration free flight (1428 slugs). It may be noted from Figure 15, that terminal flight path angle is -5.4^{o}. This compares with -4.5^{o} on the throttle fixed constrained attitude and velocity solution.

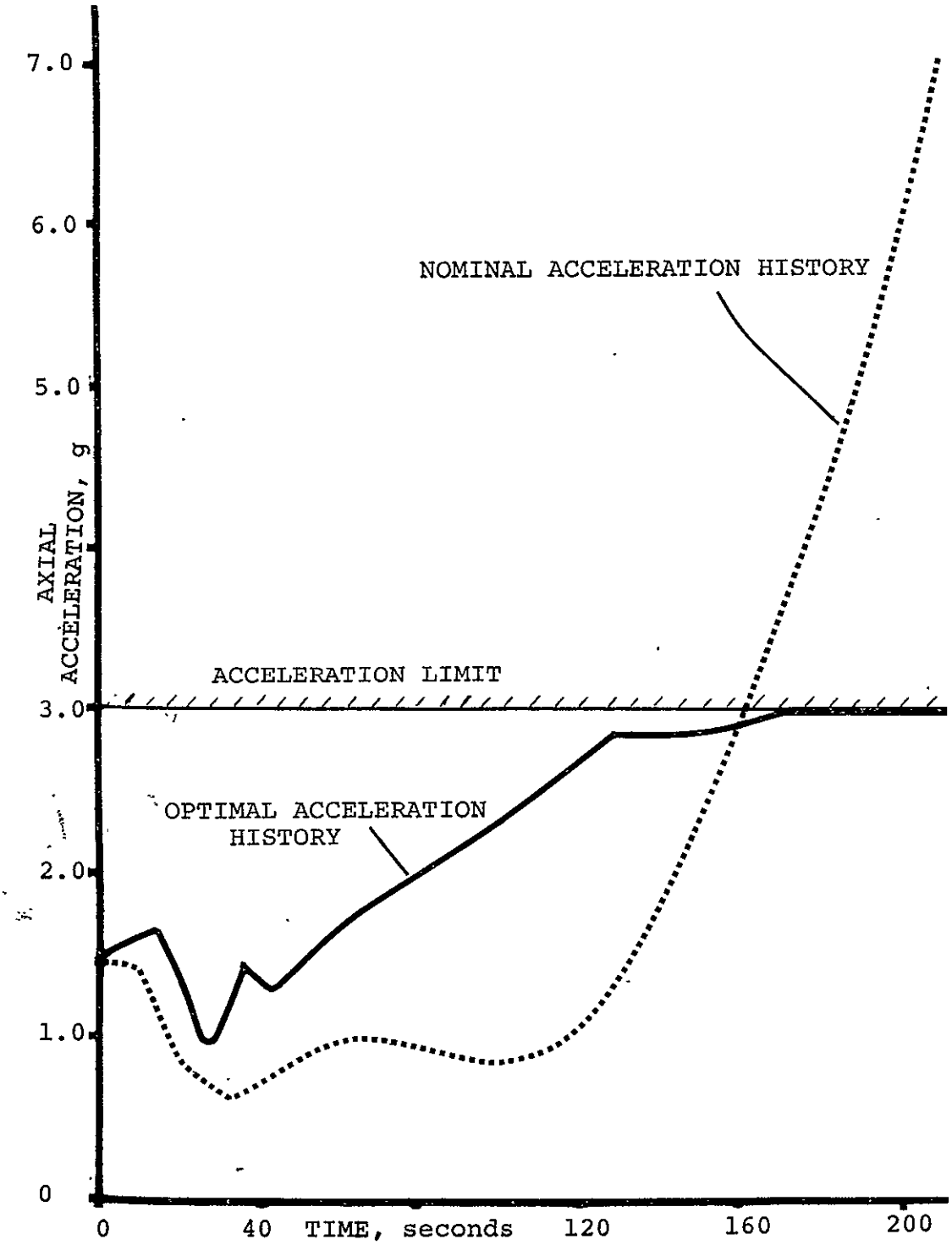

Figure 18.—HRA Maximum Mass Ascent, Acceleration History

Throttle Free Maximum Terminal Mass Ascent with In-Flight Inequality Constraints on Axial Acceleration, Altitude, And Throttle Setting

The most complex ascent path determined in the study was a maximum terminal mass ascent with terminal altitude, velocity, and flight path angle constrained together with in-flight inequality constraints on axial acceleration, altitude, and throttle setting employing two control variables. Symbolically,

$$\phi = -M; \quad \psi = h, V, \gamma, h(t), A_x(t), N(t); \quad \alpha = \alpha(t), N(t)$$

This creates a problem requiring eight state variables and six terminal constraints. As in previous HRA ascent paths, velocity is employed as the cut-off function and, hence is always satisfied. Constraint equations follow.

$$\begin{aligned} h &= 119{,}300 \\ V &= 12{,}456 \\ \gamma &= 0.0 \\ A_x(t) &\leq 3.0 \\ h(t) &\leq 120{,}000 \\ N(t) &\leq 1.0 \end{aligned}$$

Convergence behavior is presented in both tabular and graphic fashion in Table IV and Figure 19, respectively. The optimal ascent profile has been included in Figure 14. Terminal mass achieved is 1393 slugs. The decrease of 33 slugs recorded over the immediately preceding solution must be attributed to imposition of the level flight and maximum in-flight altitude constraints.

The final flight path obtained, Figure 14, is similar in character to the full throttle ascent obtained with comparable constraints. Hence, as in this previously obtained solution, it appears reasonable to surmise that the major portion of the performance degradation in the present solution is attributable to the altitude inequality constraint. Total flight time from lift-off to acquisition of desired terminal state is 200.5 seconds, approximately two seconds less than the optimal path obtained without the level flight and altitude inequality constraints. Convergence, Figure 19, is well behaved. Twenty-eight iteration cycles effectively determine optimal constrained performance. As in all previous HRA trajectories, performance convergence is characterized by small initial gains, followed by a period of more rapid performance gains and finally a series of small performance adjustments to account for constraint satisfaction. The result is an S-shaped performance convergence history. This typical shape results from the step-size logic embodied in the program of References 1 and 2.

Constraint convergence is somewhat more varied. Here terminal altitude, flight path angle, and throttle inequality constraint exhibit a convergence pattern similar to that of performance. The remaining two inequality constraints initially are subject to progressively increasing violations before final regular convergence to the desired values.

TABLE IV.— HRA THROTTLE FREE ASCENT CONVERGENCE DATA

Cycle	ϕ	ψ_1 (h)	ψ_2 (γ)	ψ_3 ($\int \Delta A_x dt$)	ψ_4 ($\int \Delta h dt$)	ψ_5 ($\int \Delta N dt$)
0	997	155400	10.04	88.1	305864	0
1	1011	155478	9.95	87.0	321118	.281
2	1004	154277	10.36	85.0	319216	.655
3	1006	153995	10.41	83.3	334159	.838
4	1013	153626	10.33	81.5	350887	1.00
5	1047	153038	10.32	79.8	369256	1.54
6	1060	152860	10.00	77.3	405941	1.48
7	1091	151916	9.64	73.8	447957	1.43
8	1148	148803	9.26	68.7	494304	1.39
9	1193	141697	10.88	66.5	307619	1.61
10	1236	137801	9.71	60.4	301230	1.47
11	1269	134832	7.87	53.5	335290	1.26
12	1293	133072	6.44	48.1	371281	1.09
13	1313	131900	5.17	43.2	413404	.948
14	1332	131029	3.98	38.3	461297	.807
15	1349	130453	2.86	33.4	517511	.668
16	1364	130080	1.80	28.1	583089	.531
17	1377	129742	.781	21.8	662943	.390
18	1389	131271	.320	18.9	773705	.316
19	1395	130182	.059	15.7	784013	.286
20	1401	127235	-.371	10.7	745923	.277
21	1401	121884	-.315	6.59	487855	.234
22	1402	120257	-.103	4.56	305344	.216
23	1398	120487	-.033	3.26	170192	.095
24	1398	119957	-.036	2.29	99380	.062
25	1396	119353	.020	1.44	39877	.042
26	1393	119438	.005	1.00	13137	.0009
27	1392	119308	.004	.721	4349	0.0
28	1393	119478	-.005	.323	4951	.003
29	1392	119289	-.001	.262	1058	.002
30	1393	119349	.003	.014	627	.036
31	1393	119299	-.0004	.013	207	.014

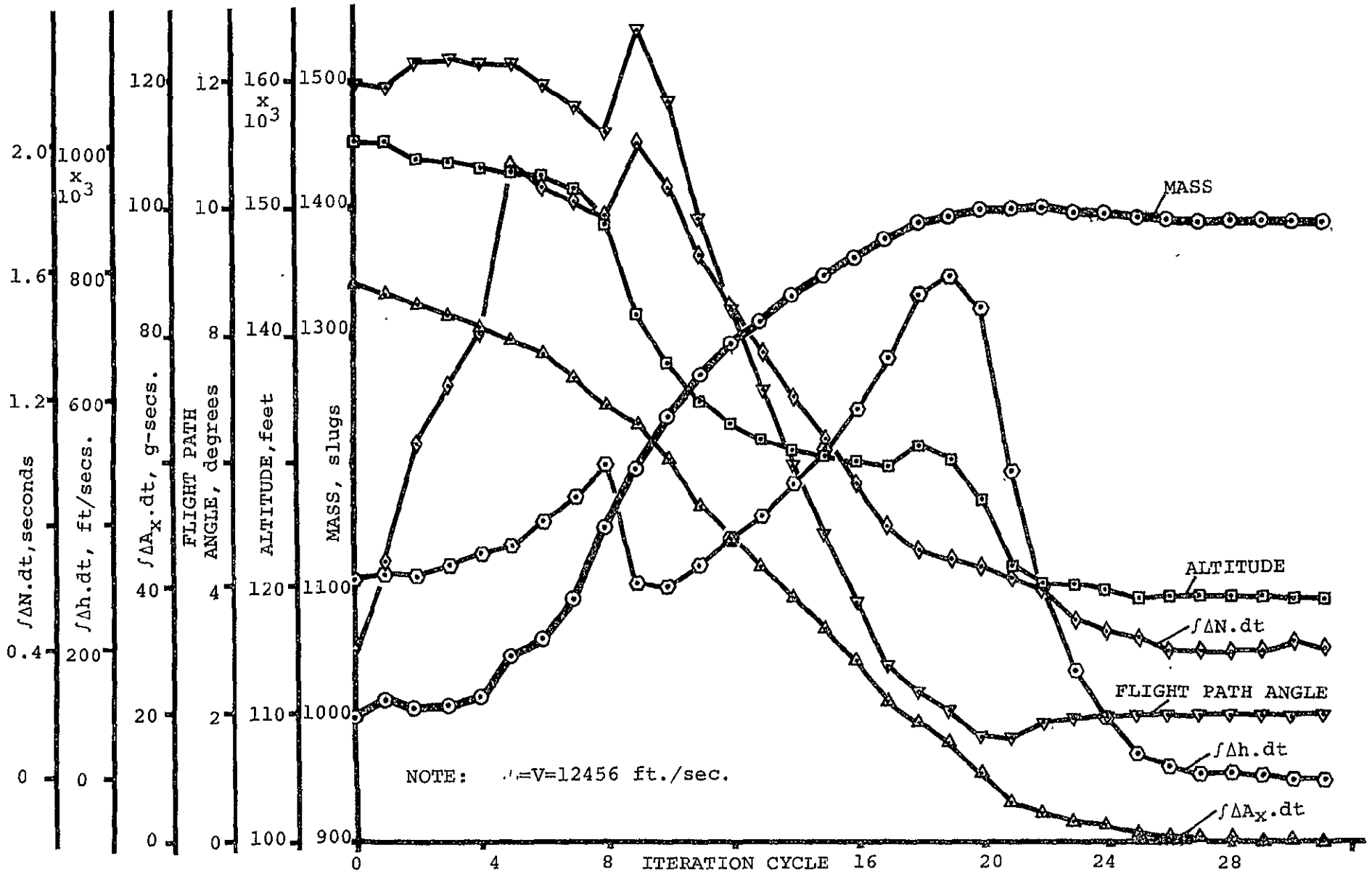

Figure 19.—HRA Throttle Free Ascent, Convergence Plot, Six Constraints

HYPERSONIC RESEARCH AIRCRAFT RETURN TRAJECTORIES

Return-to-Base Configuration

In the studies of this report, the HRA return-to-base is performed with engines off. Vehicle aerodynamic characteristics are strongly affected by the engine-off condition. The most significant change appears as an increase in the vehicle zero-lift drag due to high engine-off base drag. The drag increment is Mach number dependent, as illustrated in Figure 20.

From the performance estimation standpoint, return-to-base trajectory shaping can be expressed in terms of the ground "foot print" attainable from state conditions at descent commencement. In subsequent HRA trajectories the vehicle descent commences at

h = 119,300 feet
V = 12, 456 ft./sec.
γ = 0.0 level flight
M = 1364.6 slugs
R = 0, N.M.

The scope of the present study was limited to planar HRA trajectories. Hence, the maximum and minimum range trajectories are required.

Maximum range trajectories are computed on the basis of engine off-drag characteristics and initial state described above. Minimum range trajectories are performed with deployment of a controllable speed-brake capable of producing the additional Mach dependent drag increment of Figure 21. In the present studies, this device is assumed to be fully extended. Hence, the minimum range vehicle characteristics consist of basic HRA aerodynamics as used in the ascent trajectories, together with the engine-off and speed brake drag increments.

Maximum Range Return Angle-of-Attack Control

Maximum range return trajectories were computed from the nominal control history of Figure 22. This linearly decreasing control history generates the velocity altitude flight profile of Figure 23. An initial zoom to approximately 180,000 feet is followed by three "skip-like" maneuvers of decreasing energy. Below a velocity of 4000 ft./sec., energy decreases smoothly and rapidly until an altitude of 40,000 feet is achieved. At this point a marked change in flight path becomes apparent. Above 40,000 feet, the trajectory is almost normal to the specific

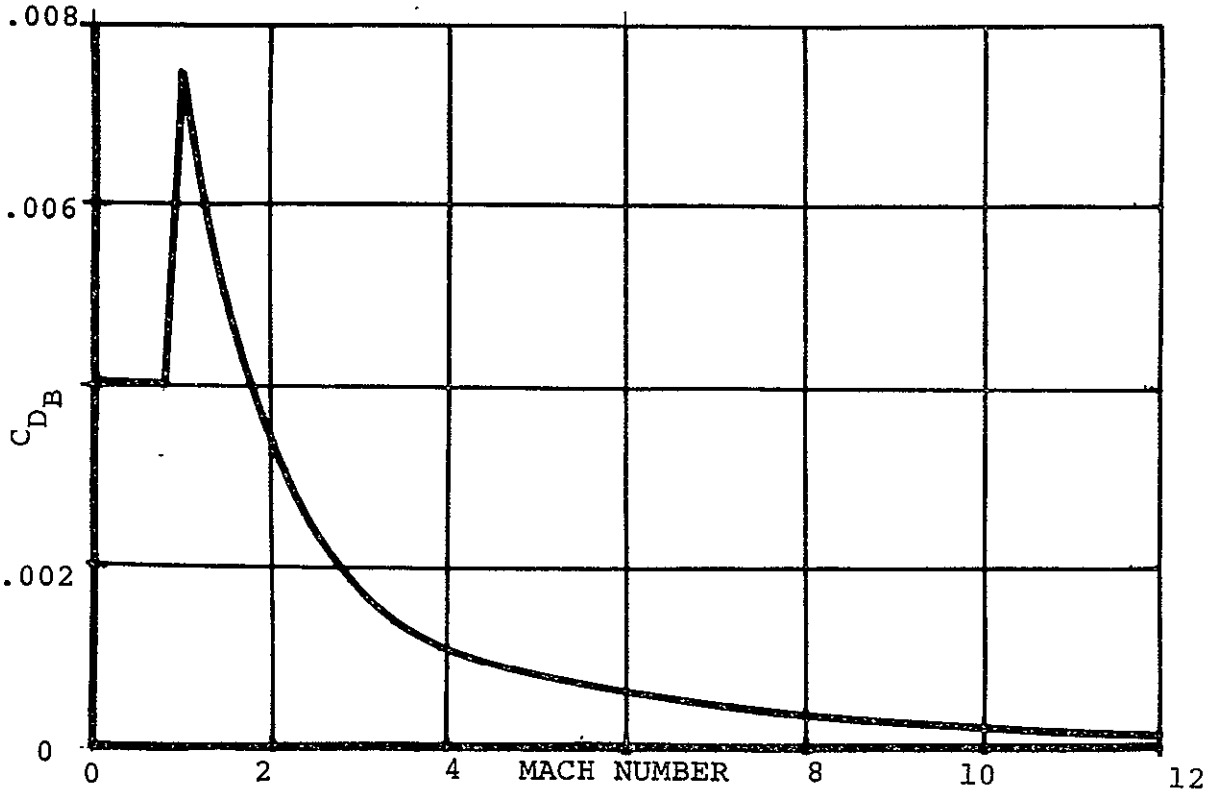

Figure 20.—HRA Engine-Off Drag Increment

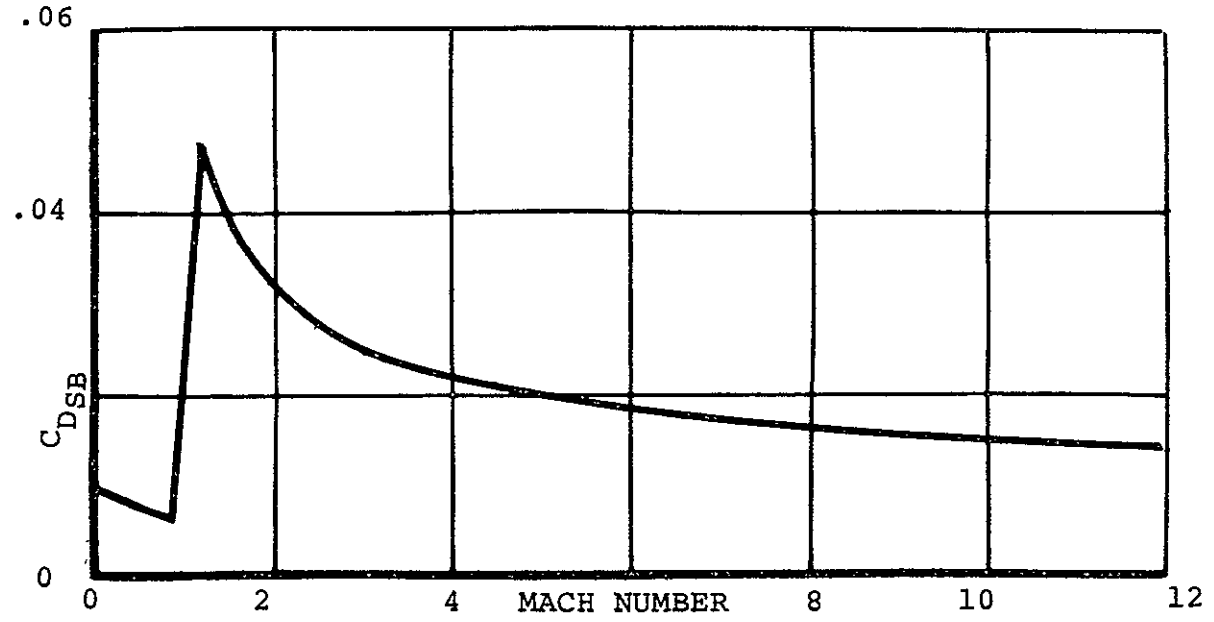

Figure 21.—HRA Full Speed-Brake Drag Increment

energy contours; below 40,000 feet, the trajectory is aligned more closely with the energy contours.

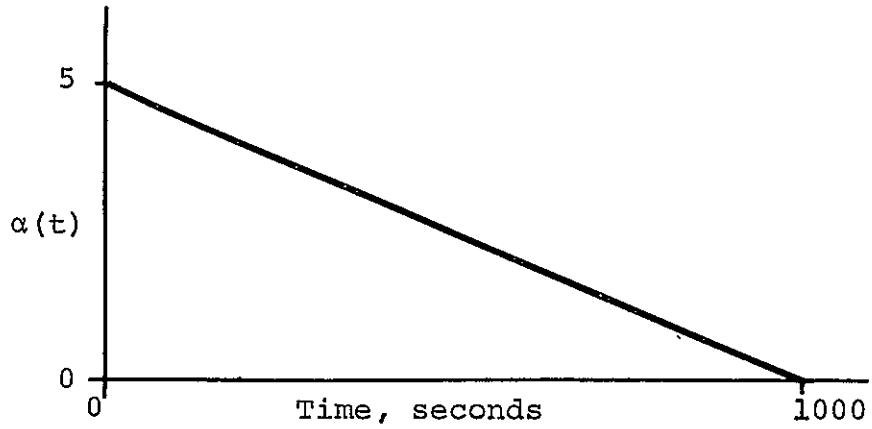

Figure 22.—Nominal Angle-of-Attack History, HRA Maximum Range Return

The optimization problem studied was that of maximizing longitude, θ_L, at a terminal altitude of 3000 feet. Symbolically,

$$\phi = \theta_L, \ \Omega = h; \ \alpha = \alpha(t)$$

The single constraint, terminal altitude, must be employed as cut-off function. The final trajectory attained is presented in Figure 24. The initial zoom exceeds an altitude of 200,000 feet. It is followed by six skip-like maneuvers before a smooth decay of energy occurs. Terminal range achieved is 1582 nautical miles corresponding to a longitude of 26.32 degrees at the equator.

Convergence behavior is presented in Table V. Initially, large performance gains are achieved at each iteration. Terminal convergence is slow, however, and at the calculation termination performance gains of 0.1 degrees of latitude per iteration were still being achieved. Slow terminal convergence of long duration trajectories is often experienced with angle-of-attack control. On such trajectories angle-of-attack control will frequently produce a flight path of an oscillatory nature due to the ease with which "phugoid-like" motion can be developed. In the case of the present trajectory which has a duration of 1583 seconds, there is ample time available for the development of oscillatory flight.

In the present solution, the significance of the oscillatory flight-path is not clear. A detailed analysis, possibly using

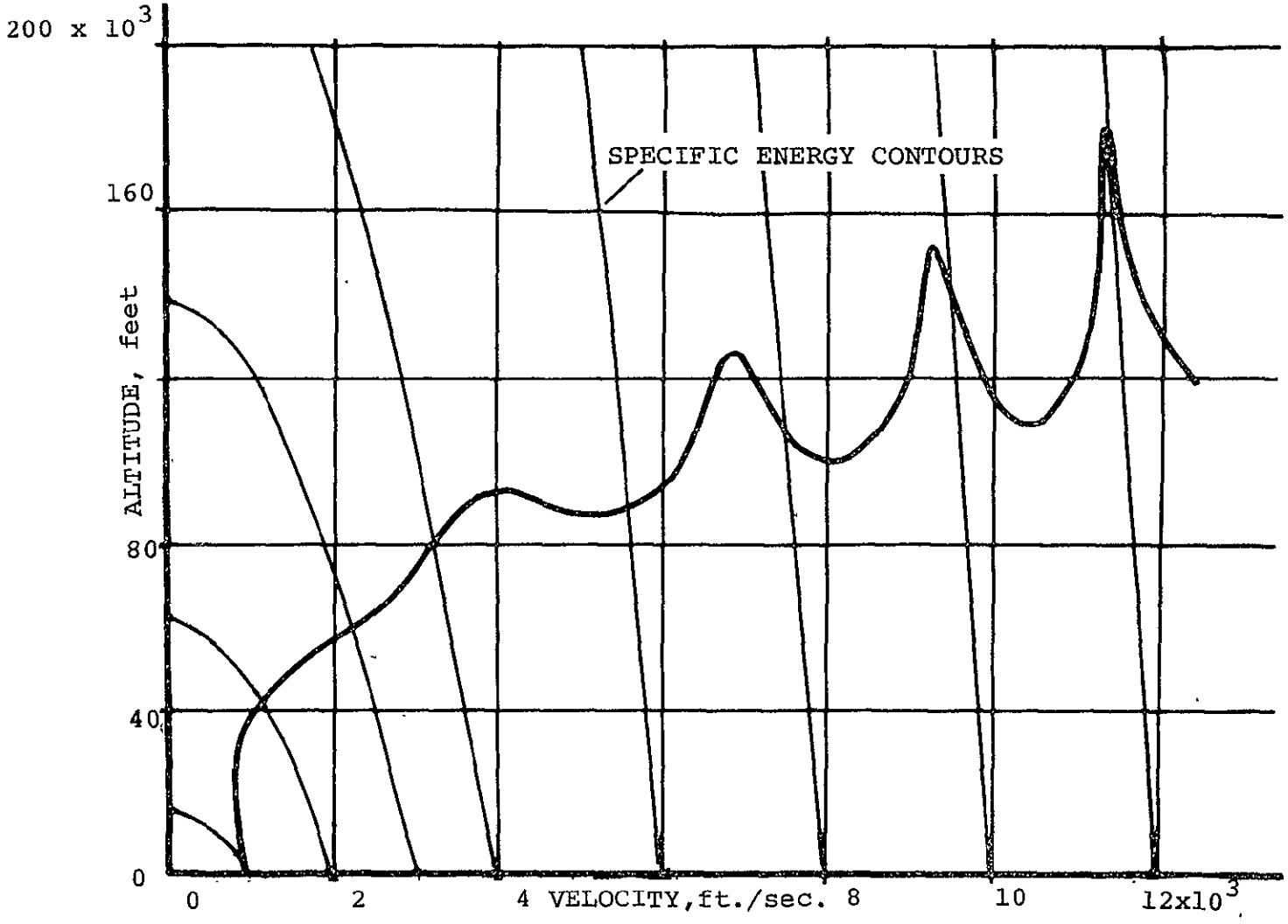

Figure 23.—Nominal Path, HRA Return Trajectory

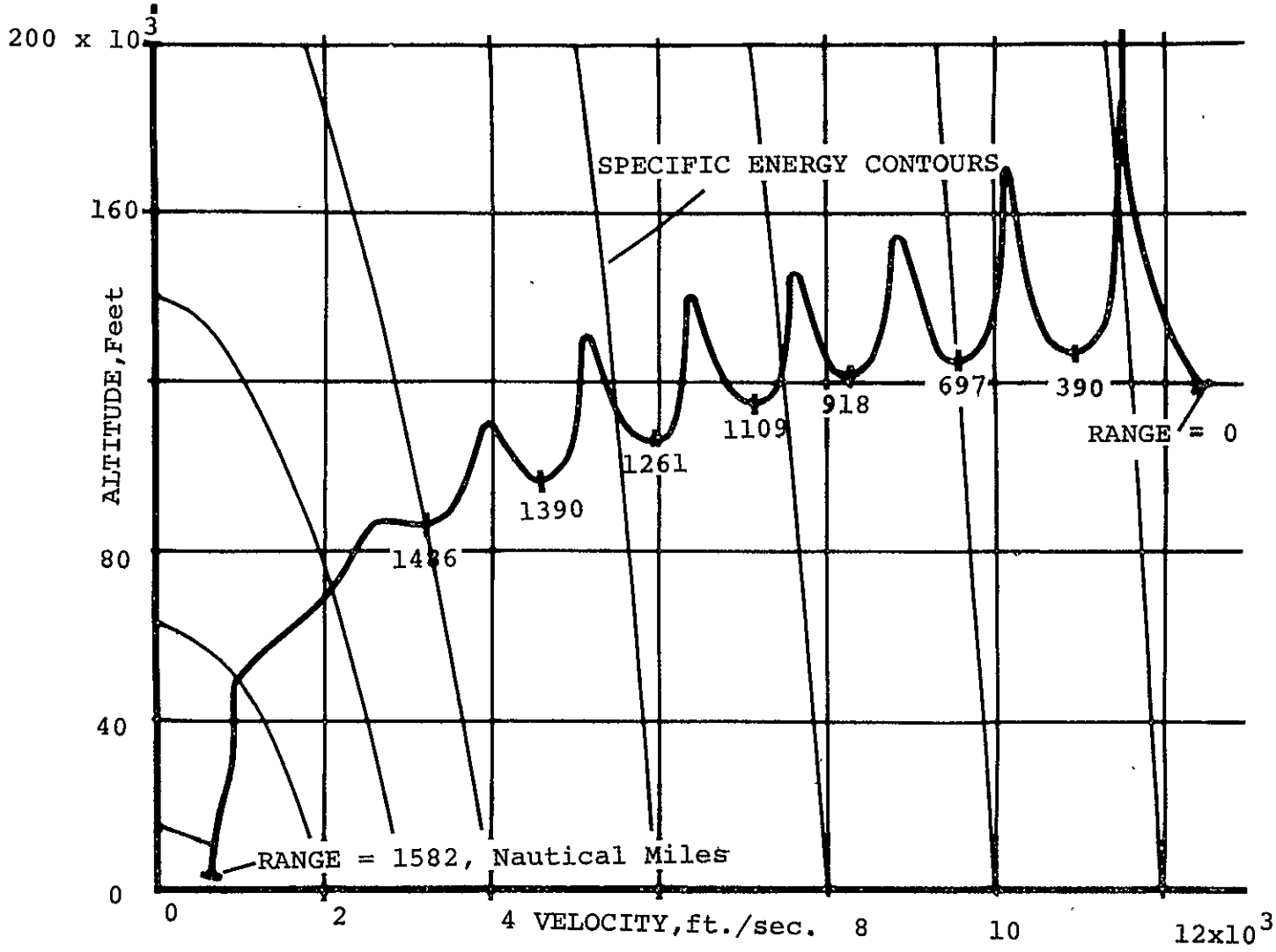

Figure 24.—HRA Maximum Range Return Trajectory, Angle-of-Attack Control

the quasi-steady reasoning of Reference 9 might cast light on the physical significance of the motion; such an analysis lay beyond the scope of the present study.

TABLE V.—

CONVERGENCE BEHAVIOR, HRA MAXIMUM RANGE TRAJECTORY WITH ANGLE-OF-ATTACK CONTROL

Iteration Cycle	$\phi(\theta_L)$
0	16.39
1	20.08
2	21.21
3	22.43
4	23.26
5	24.11
6	24.60
7	24.91
8	25.17
9	25.45
10	25.60
11	25.78
12	25.90
13	26.04
14	26.11
15	26.23
16	26.32

Maximum Range Return, Pitch Angle Control

A Hypersonic Research Aircraft maximum range return path was also computed using vehicle pitch angle history as the control variable. This calculation was performed in order to assess the oscillatory flight path developed in the preceding section and to compare convergence behavior with the two pitch plane controls.

Pitch angle control was originally introduced into the program of Reference 1 in the study of hypersonic cruise aircraft trajectories reported in Reference 10. Pitch control is readily added to this program in the manner described in Appendix A.

For the present mission, some difficulty was experienced in generation of a nominal path by means of pitch control. With angle-of-attack control in the preceding section, an integration step of $\Delta t = 8$ seconds was employed. With pitch control the equations of motion become numerically unstable at low altitude with this step-size; accordingly, the present calculation commenced with a step-size of $\Delta t = 2$ seconds. The fixed step Runge-Kutta integration technique was employed. With this step the nominal pitch history of Figure 25 produced a readily integrated flight path. After five iterations an attempt to continue the calculation with an eight-second integration step again resulted in a numerically unstable trajectory integration at low altitude. The eight-second step-size was retained, however, and the terminal cut-off condition was changed from the previously employed $h = 3000$ feet to $h = 40{,}000$ feet. This modification to the problem statement avoided further numerical difficulties. Table VI presents convergence behavior. It can be seen that at cycle 5, where the integration step-size and terminal altitude are modified, a distinct jump occurs in payoff function convergence. This jump is due almost entirely to the change in integration step, for the change in terminal altitude from 3000 to 40,000 feet produced only .04 degrees of longitude change in performance on the two-second integration step path.

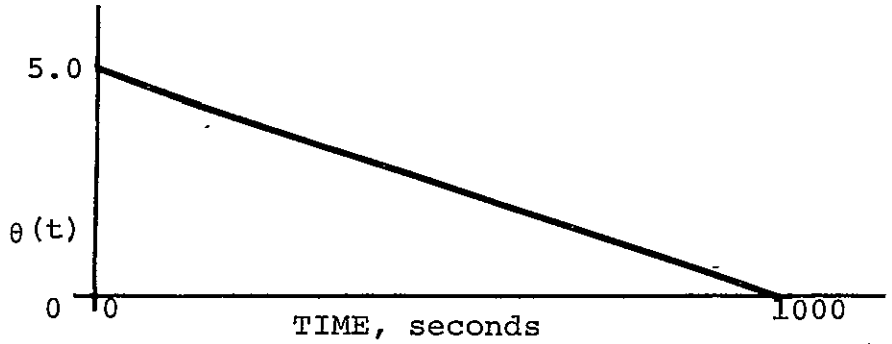

Figure 25.—Nominal HRA Maximum Range Pitch History

TABLE VI.—
HRA MAXIMUM RANGE CONVERGENCE, PITCH ANGLE CONTROL

Iteration Cycle	$\phi(\theta_L)$	Δt
0	7.58	2.0
1	12.41	2.0
2	16.63	2.0
3	20.33	2.0
4	23.20	2.0
5	25.15	2.0
5	24.35	8.0
6	25.50	8.0
7	26.11	8.0
8	26.35	8.0
9	26.52	8.0
10	26.62	8.0
11	26.65	8.0
12	26.70	8.0
13	26.72	8.0

Three of the trajectories obtained in the maximum range pitch control study are presented in Figure 26. The nominal path generated by the straightforward control history of Figure 25 descends rapidly without skipping. After five iteration cycles, a skip-like maneuver has developed, and range has increased from an initial 7.58 degrees of longitude to 25.15 degrees longitude (Table VI). Subsequently, with the eight-second integration step discussed above, a range of 26.72 degrees of longitude is achieved after 13 iterations. This value is slightly greater than the range of 26.32 degrees of longitude (Table V) achieved with angle-of-attack control. It can be seen that little change occurs in the initial portion of the flight path between the fifth and thirteenth iterations. At lower Mach numbers the flight path has risen in altitude, however, and the smaller skip-like motions have become somewhat more pronounced. The final path obtained with pitch control lies fairly close to the mean path obtained by smoothing the skips of the angle-of-attack solution. Thus, it appears that the multiple skips encountered with angle-of-attack control have little physical significance. They are presumably introduced by angle-of-attack dynamics which readily introduce phugoid-like motions. The initial skip, which is used to acquire a more favorable Mach-altitude point than the initial state provides, does appear to be physically significant since it is found with either type of control.

Minimum Range Return Without Acceleration Limit

An acceleration free minimum range return to base was computed to establish a lower limit on HRA range capability. Minimum range maneuvers tend to have a highly dynamic nature; hence, the possibility of flight through the vertical condition must be considered. The trajectory optimization program of Reference 1 will perform planar maneuvers which pass through the vertical provided that the vehicle control variable bank-angle B_A is defined in a state-dependent manner as a function of vehicle heading, σ. In planar motion flight through the vertical implies a heading angle reversal. At each such reversal the bank-angle is rotated by 180°, retaining positive g force on the aircraft pilot. Thus, in an Immelman Turn (the first half of a loop), the initial zero bank-angle becomes 180° as the vehicle passes through the vertical. In a Split "S" maneuver (the first half of a reverse loop), the vehicle is initially rotated through 180°; as the vehicle passes through the vertical, a zero degree bank condition is assumed.

State dependent vehicle control can be specified in the program of Reference 1 through the Flight Plan Program Options. These options permit tabular definition of any control variable as an arbitrary function of vehicle state. For HRA minimum range acceleration paths,the possibility of development of a Split "S" (tuck under) maneuver was considered.

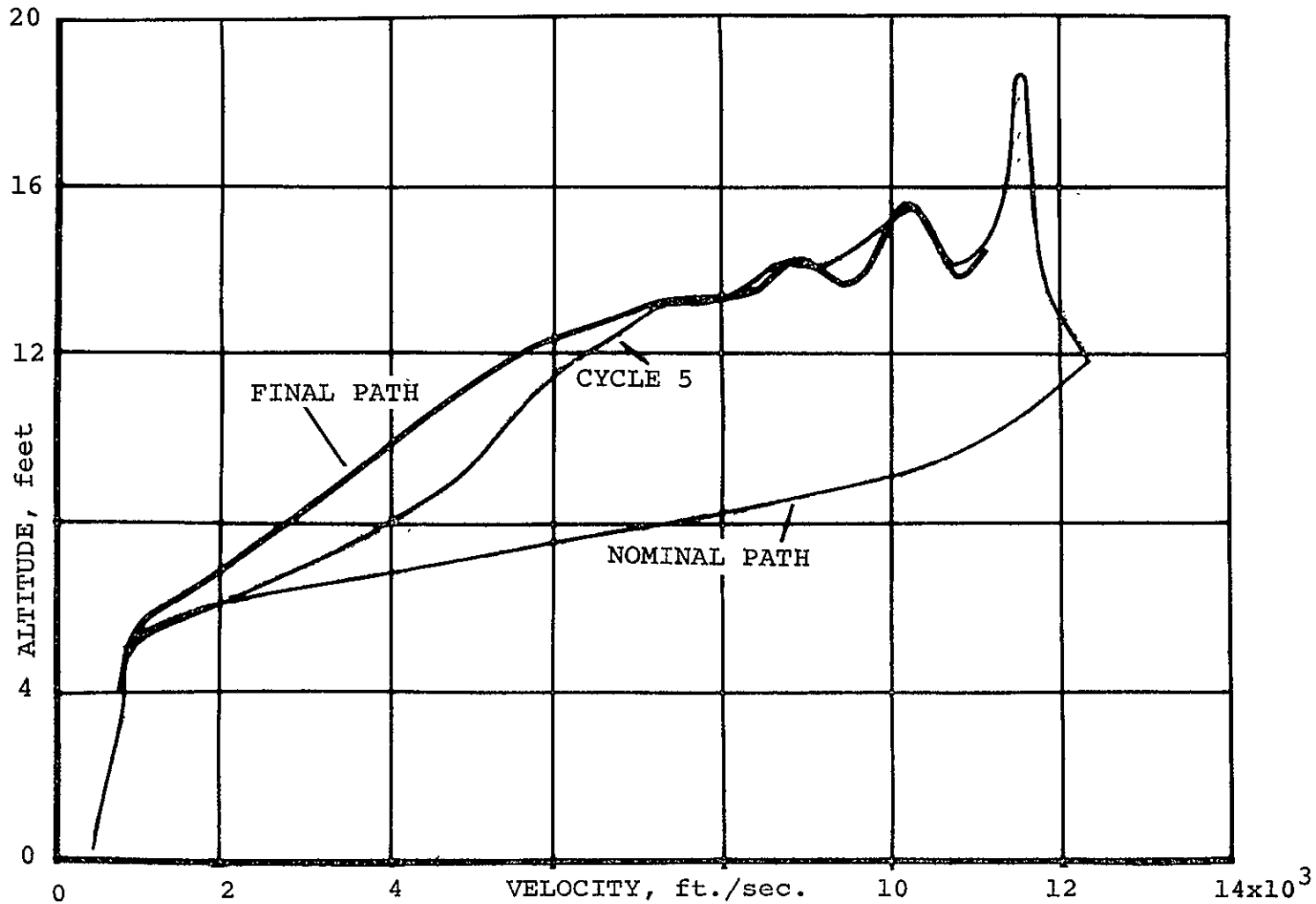

Figure 26.— HRA Maximum Range Trajectory, Pitch Control Solution

Accordingly, the bank-angle state-dependency of Figure 27 was imposed. It may be noted that the HRA drag polar is symmetric about the zero lift condition; hence, the assumption of initial inverted flight at some positive angle-of-attack provides an identical force system to upright flight with a change in sign on angle-of-attack.

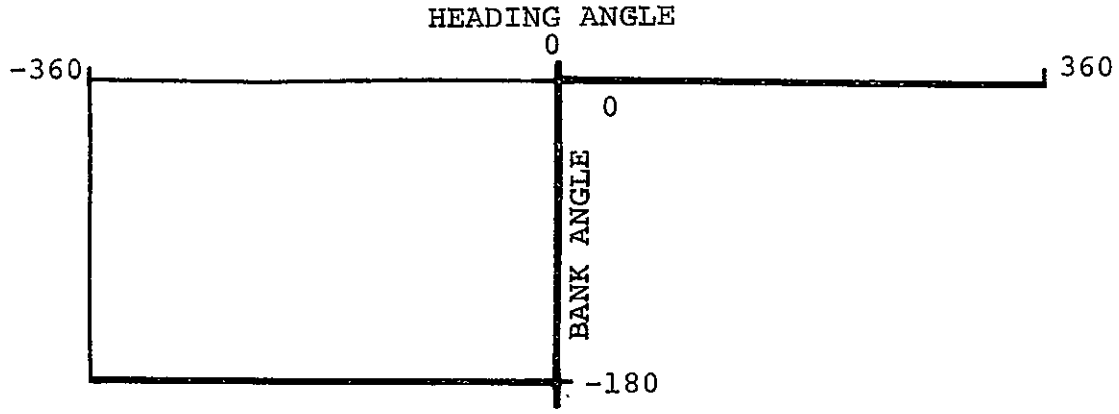

Figure 27.—State Dependent Bank Angle

Solutions were obtained from two nominal paths: one employing zero lift and the other a linearly decreasing angle-of-attack. Each solution was pursued for nine iteration cycles with the results presented in Table VII. It may be noted that range minimization was achieved by longitude minimization. Ranges of .33 and .36 degrees were achieved in these calculations. Since the maneuvers involve extremely high accelerations, in excess of one hundred "g," no attempt to define the extremal with more precision was undertaken.

Nominal and final paths are presented in the altitude-longitude plane in Figure 28; it may be noted that the vertical scale is exaggerated. The well-separated nominal paths converge to quite similar final paths in this plane. Separate velocity-altitude profiles are presented for each solution in Figures 29 and 30. It can be seen from Figure 28 that following the Split "S" which produces a heading reversal, the vehicle assumes a glide condition seeking to minimize range by gliding as far as possible towards the initial point or beyond.

Minimum Range Return, Acceleration Limited

In this study, a minimum range trajectory subject to an acceleration limit of 3g at all points along the path was computed. The acceleration limit is placed on total g experienced by the vehicle. The zero-lift nominal path of the previous section was employed in the calculation. Convergence details

TABLE VII.—MINIMUM RANGE HRA TRAJECTORY CONVERGENCE

Iteration Cycle	Longitude (Degrees)	
	Zero Lift Nominal	Linear α Nominal
0	2.464	4.713
1	1.669	2.264
2	1.009	1.372
3	.868	1.094
4	.659	.792
5	.635	.357
6	.597	.332
7	.567	.330
8	.390	.328
9	.356	.327

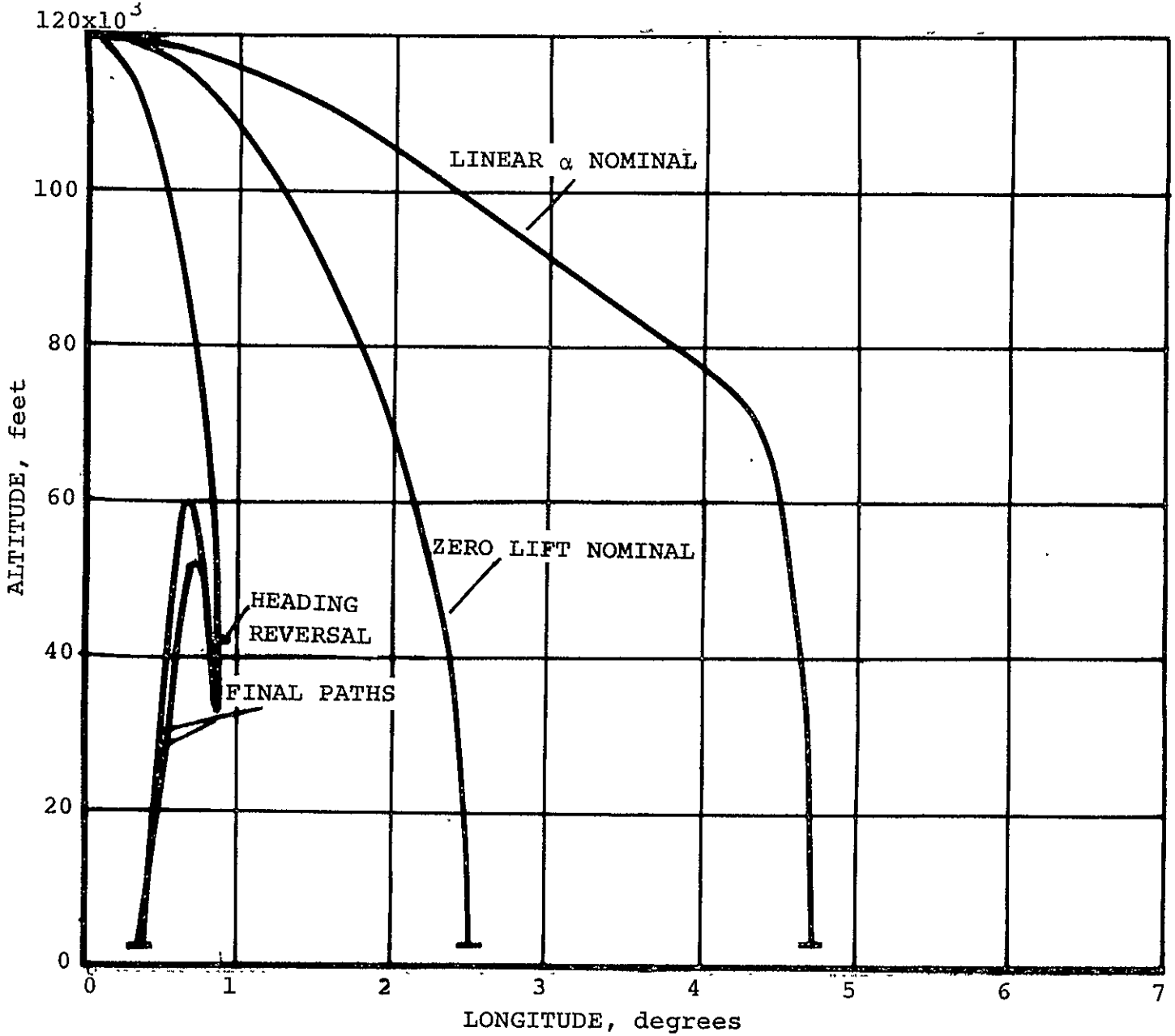

Figure 28.—HRA Minimum Range Trajectories, Altitude vs. Longitude

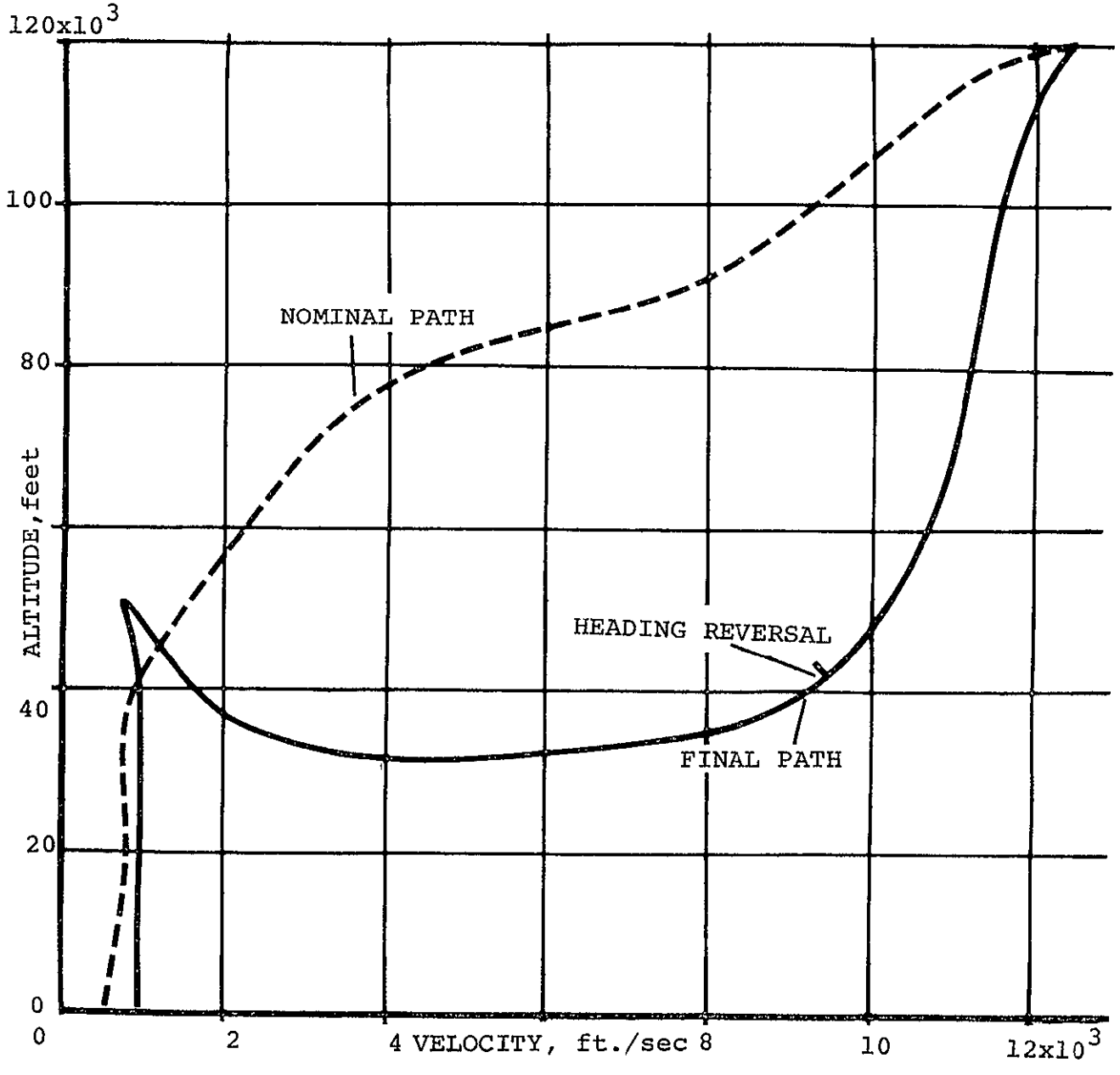

Figure 29.—Minimum Range HRA Return Trajectory--Linear Nominal Control

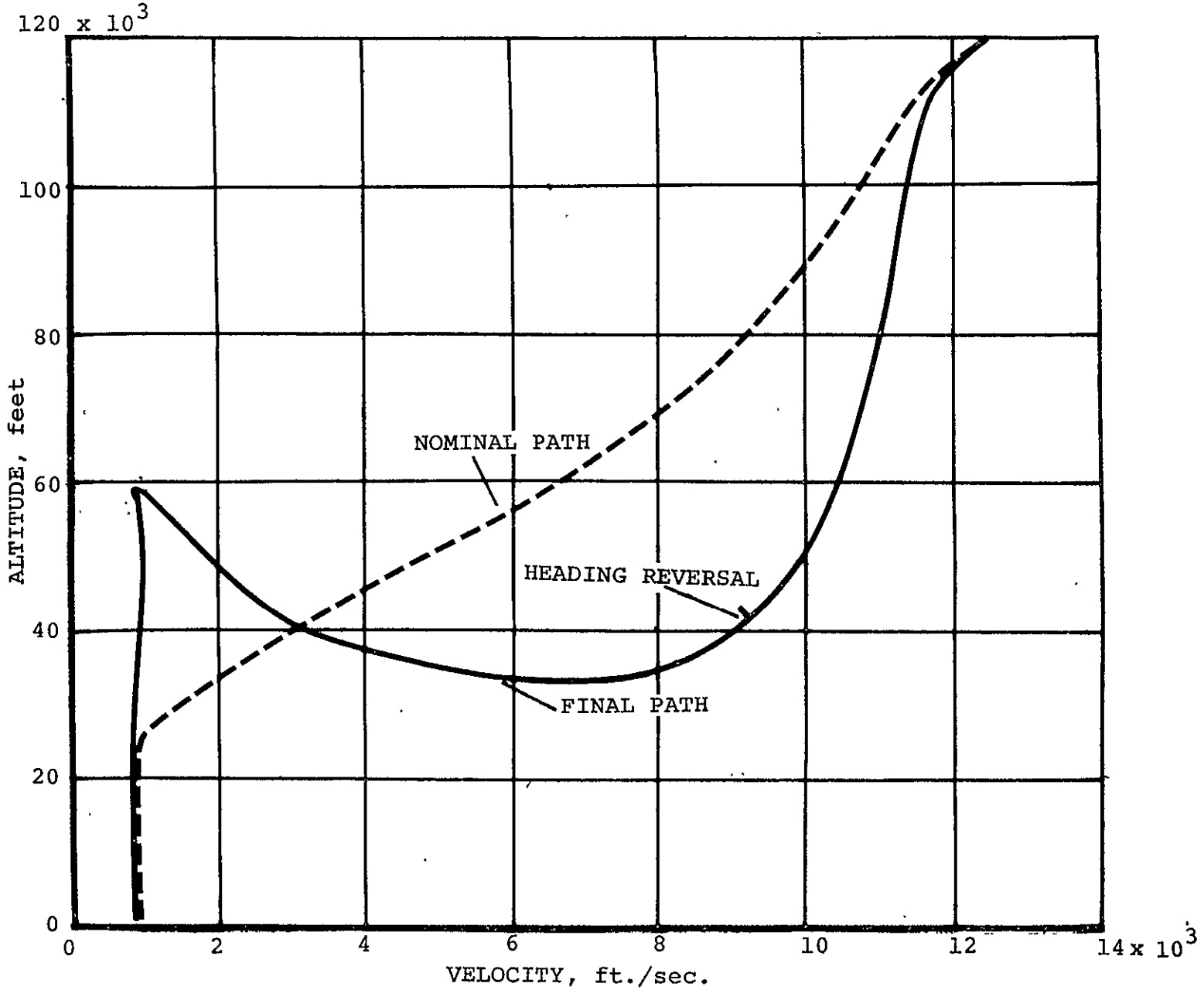

Figure 30.—Minimum Range HRA Trajectory - Zero Lift Nominal

are presented in Table VIII. Since the minimum range acceleration limited solution was considered unlikely to develop a Split "S" maneuver, a terminal constraint of minus ten degrees was imposed on the flight. Without such a constraint, the trajectory would tend to the vertical at flight termination. Symbolically, the solution can be described as

$$\phi = \theta_L; \ \psi = h, \ \gamma, \ A(t); \ \alpha = \alpha(t)$$

Terminal altitude was employed as cut-off function. The final minimum range trajectory is presented in the Mach-altitude plane in Figure 31 and in the range-altitude plane in Figure 32. Trajectory segments described by a thicker line indicate flight segments lying on the acceleration limit. The acceleration history, including a display of total acceleration, axial, and normal components is presented in Figure 33. The final angle-of-attack history is given in Figure 34.

It can be seen that the acceleration constraint and possibly the flight path angle constraint prevent development of the Split "S" maneuver. Throughout most of the flight axial acceleration is the larger component of total acceleration. Two flight segments lie on the acceleration limit. The sub-arc connecting these two periods of acceleration limited flight may be associated with achievement of the flight path angle constraint. However, the reduction in axial acceleration along this sub-arc is small; hence, it is possible that this feature is due to incomplete convergence. Clarification of this point would require computation of a solution from another nominal path or detailed analysis of the terminal maneuver. Time limitations on the present study did not permit implementation of either approach.

TABLE VIII
CONVERGENCE OF HRA MINIMUM RANGE ACCELERATION LIMITED SOLUTION

Iteration	Longitude	Flight Path Angle	$\int \Delta A(t)dt$
0	2.464	-70.05	118.8
1	2.226	-61.14	121.0
2	2.091	-52.84	119.2
3	2.036	-46.36	113.0
4	2.073	-40.17	103.5
5	2.212	-19.68	85.9
6	2.182	-15.96	102.5
7	2.240	-18.98	79.3
8	2.402	-25.07	64.9
9	2.520	-22.12	66.3
10	2.684	-16.96	34.2
11	2.728	-15.26	37.6
12	2.681	-13.48	47.6
13	2.488	-46.15	63.3
14	2.385	-32.42	61.2
15	2.450	-26.95	42.8
16	2.479	-25.11	45.0
17	2.536	-16.51	34.7
18	2.582	-13.60	32.5
19	2.623	-10.84	25.6
20	2.691	-14.02	25.4
21	2.626	-10.94	26.0
22	2.714	-11.26	18.8
23	2.683	-10.75	20.9
24	2.767	-10.86	13.7
25	2.737	-10.88	14.6
26	2.805	-10.97	10.3
27	2.814	-10.83	7.5
28	2.843	-10.74	6.0
29	2.871	-11.17	3.4
30	2.884	-10.09	1.3
31	2.874	-10.56	1.7
32	2.870	-10.05	1.5
33	2.869	-10.32	1.1
34	2.866	-10.08	0.9
35	2.866	-10.09	0.9

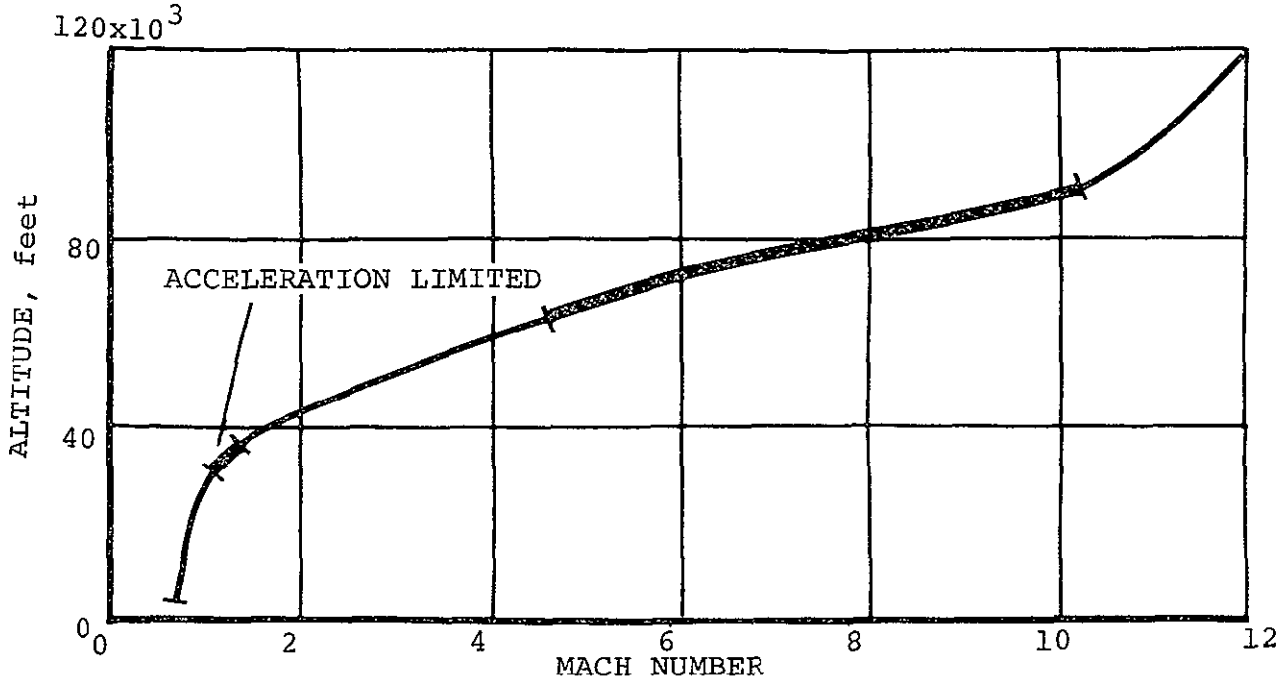

Figure 31.—HRA Minimum Range Mach-Altitude Path, Acceleration Limited

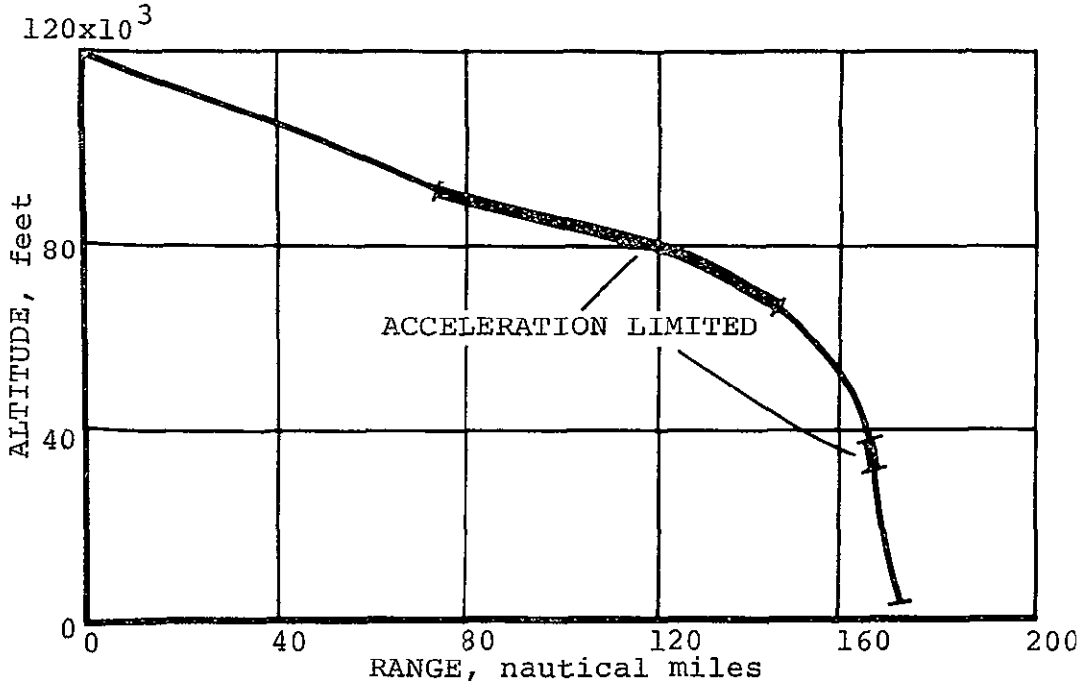

Figure 32.—HRA Minimum Range Range-Altitude Path, Acceleration Limited

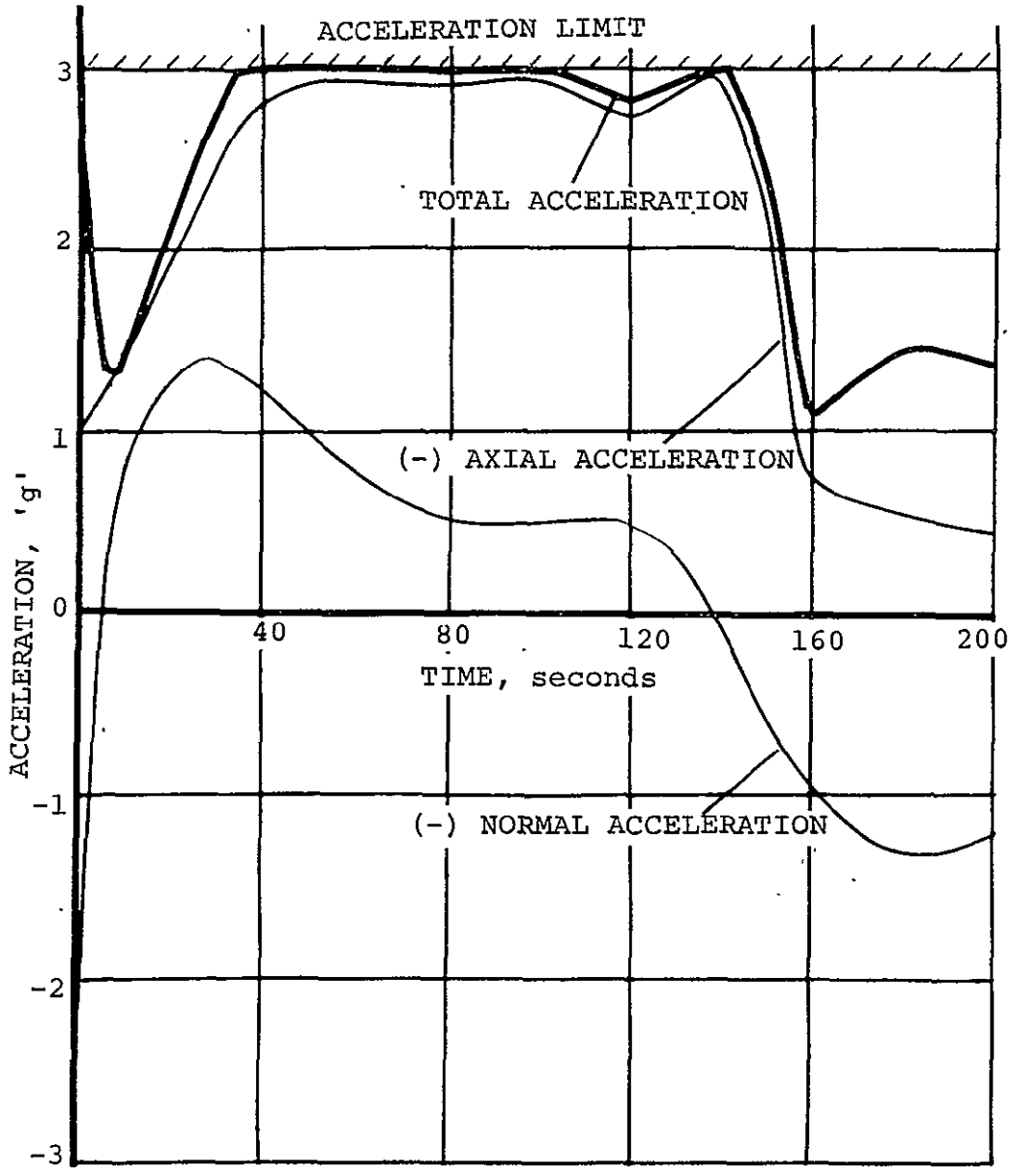

Figure 33.—Acceleration Histories, HRA Minimum Range Path

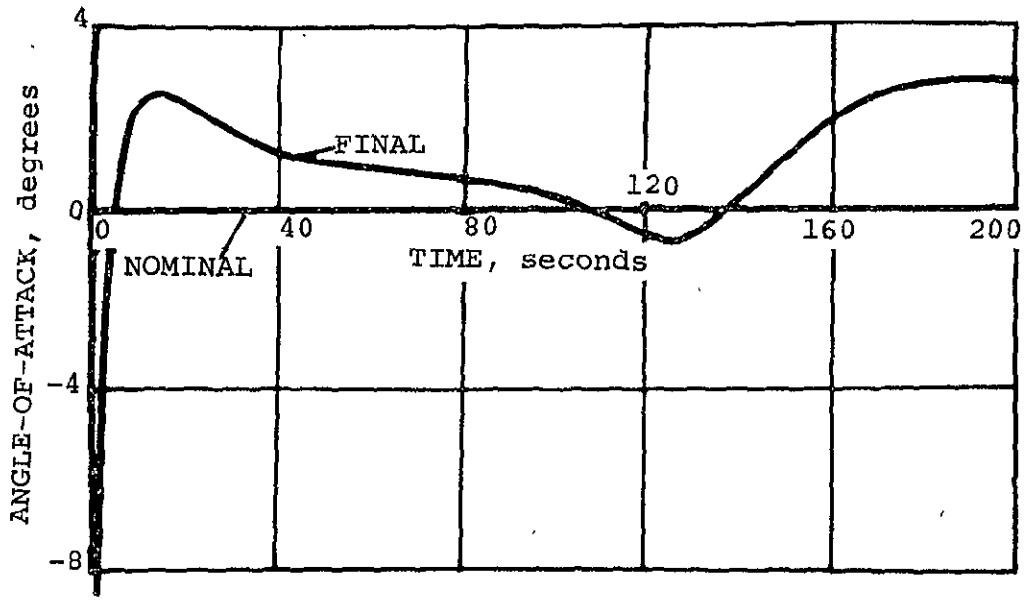

Figure 34.—Angle-of-Attack History,
HRA Minimum Range Path

SUPERSONIC TRANSPORT TRAJECTORIES

Vehicle Characteristics

A minimum fuel ascent path was determined for the aircraft configuration of Figure 35. This type of configuration has been considered as a possible supersonic transport in several feasibility studies. Aerodynamic characteristics assumed for the vehicle are shown in Figure 36. Linearized aerodynamics are assumed so that

$$C_L = C_{L_\alpha} \cdot \alpha$$

and

$$C_D = C_{D_o} + \frac{\partial C_D}{\partial \alpha^2} \cdot \alpha^2$$

$$= C_{D_o} + C_{L_\alpha}^2 \frac{\partial C_D}{\partial C_L^2} \cdot \alpha^2$$

where all coefficients are functions of Mach number as in Figure 36. In this form the data is acceptable to the program of Reference 1.

Propulsive characteristics were based on engine manufacturer's data. The functional form of the data is

$$T = T(M, h, N)$$

and

$$\dot{m} = \dot{m}(M, h, N)$$

The program of Reference 1 was modified, as described in Appendix A, to accept this propulsive data. Typical thrust and fuel flow characteristics are sketched in Figures 37 and 38 for representative throttle settings.

Minimum Fuel Ascent, Angle-of-Attack Control

A minimum fuel ascent path was computed under the assumption of maximum power. Angle-of-attack control was employed. The nominal control history of Figure 39 generated the nominal path presented in Figure 40. Symbolically,

$$\phi = m; \quad \psi = V, h; \quad \alpha = \alpha(t)$$

Convergence details are given in Table IX.

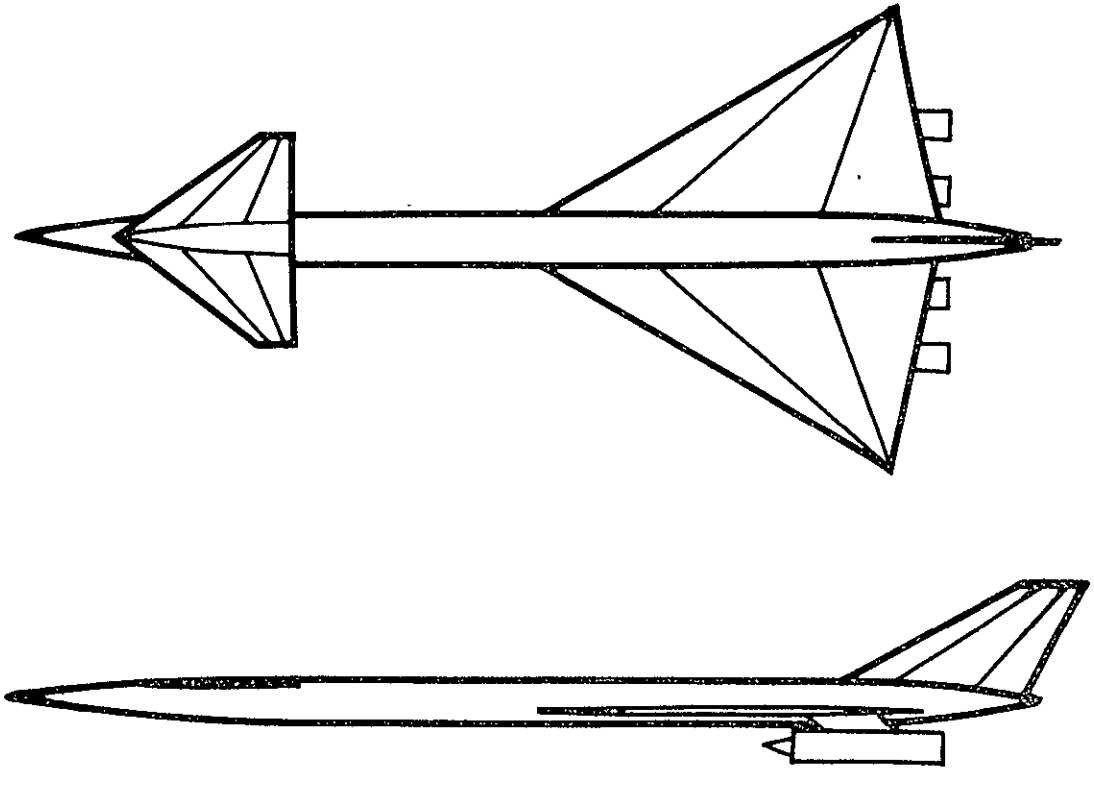

Figure 35.—Supersonic Transport Configuration

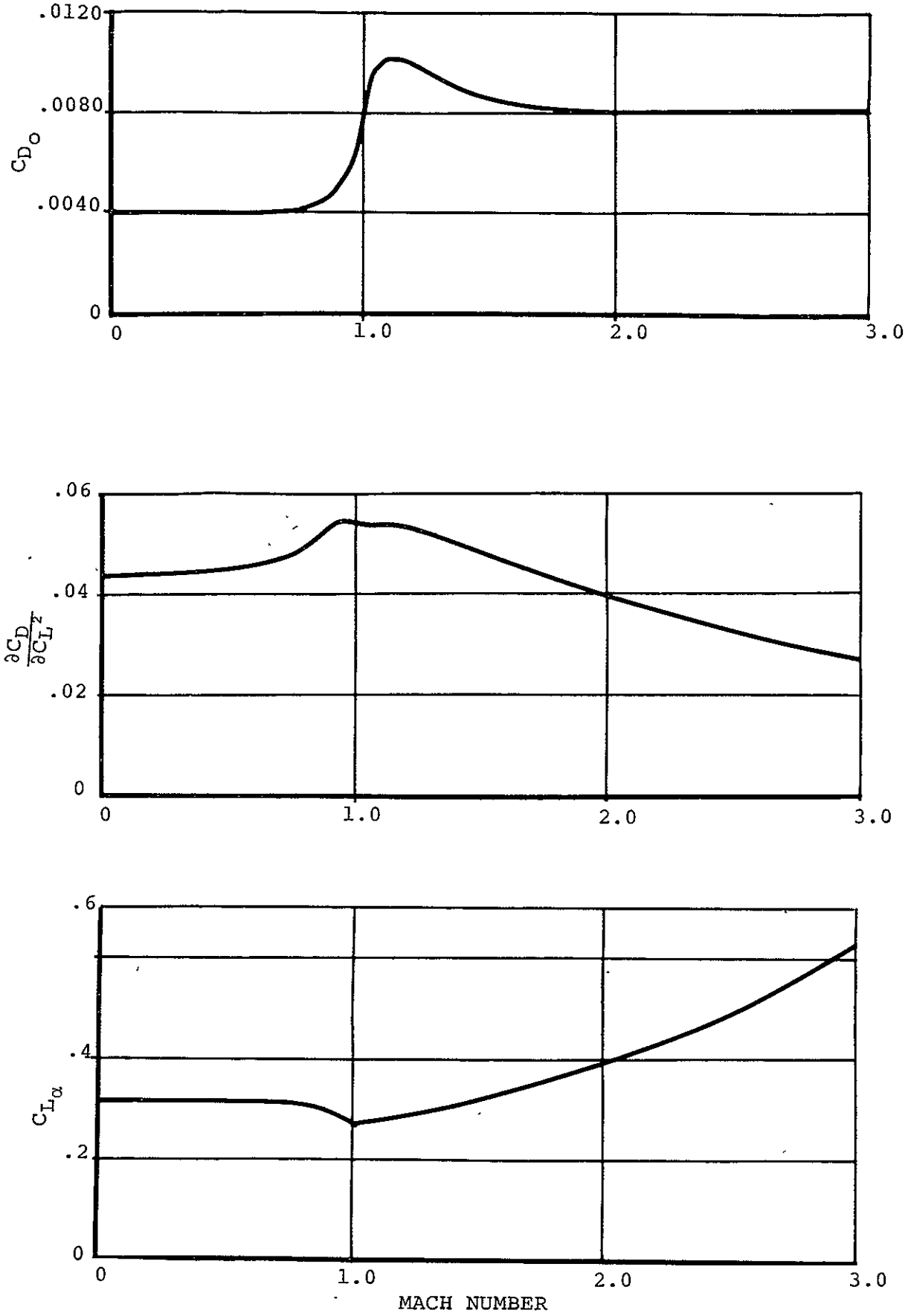

Figure 36.—Supersonic Transport Configuration Aerodynamic Characteristics

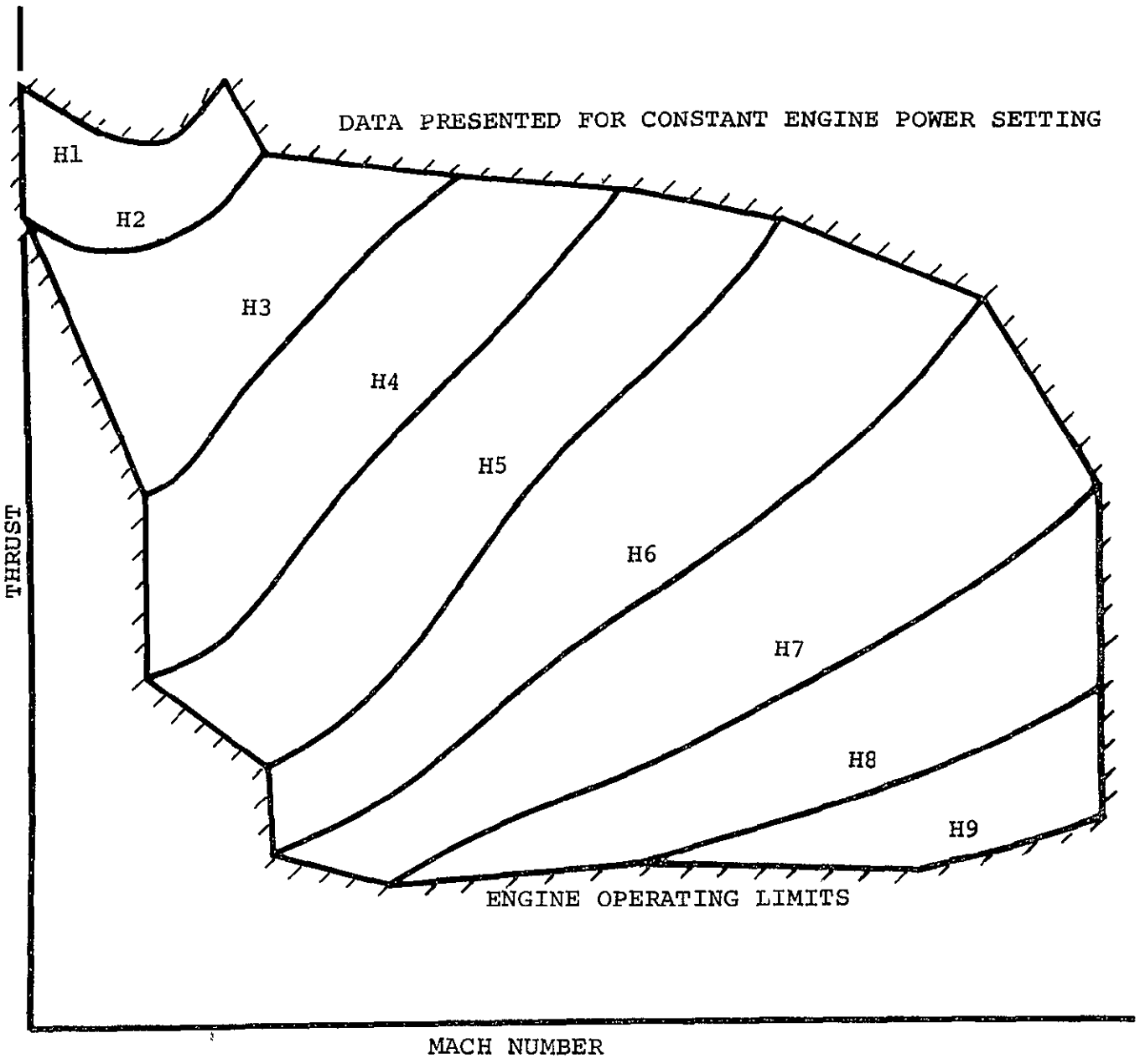

Figure 37.—Typical Thrust Data for Assumed SST Engine

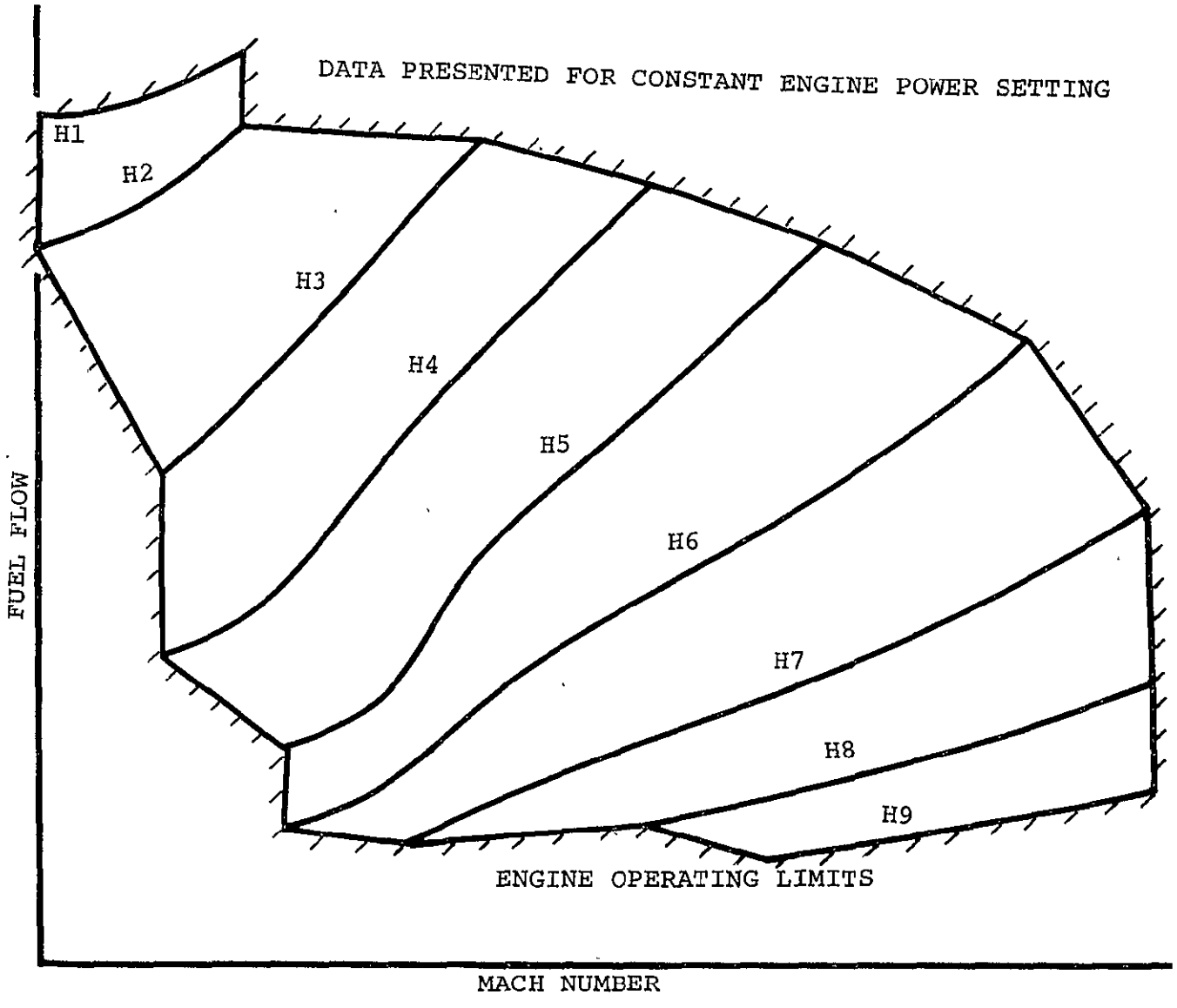

Figure 38.—Typical Fuel Flow Curves for Assumed SST Engines

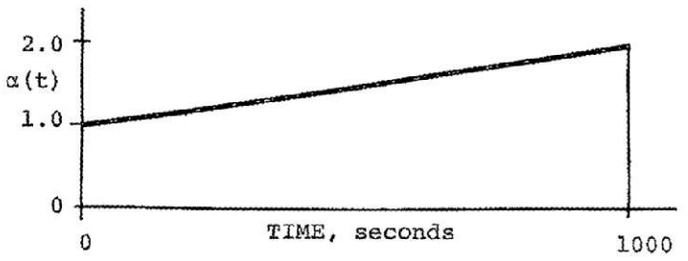

Figure 39.—Nominal SST Angle-of-Attack History

Initial conditions assumed are

Velocity, V	= 492.1 ft./sec.
Altitude, h	= 3281 feet
Flight Path Angle, γ	= 0.0
Mass, M	= 22616 slugs
Range, R	= 0

Terminal conditions desired are

V = 2625 ft./sec.
h = 63159 feet

Altitude is employed as the trajectory cut-off function and, hence, is satisfied on all trajectories.

The path developed after 28 steepest-descent iterations is shown in Figure 41. No ground plane constraint is imposed on the flight; hence, a portion of the path lies underground. Past studies have shown negligible performance changes associated with satisfaction of the ground plane constraint. Final mass of 20064 slugs results in a fuel requirement of approximately 2550 slugs. This is 11.3 per cent of the initial mass employed. Fuel required for take-off run and initial climb out is not considered in this figure. Total ascent time for this trajectory is 1114 seconds; complete terminal state is tabulated below.

V = 2626 ft./sec.
h = 63159 feet
γ = 3.3 degrees

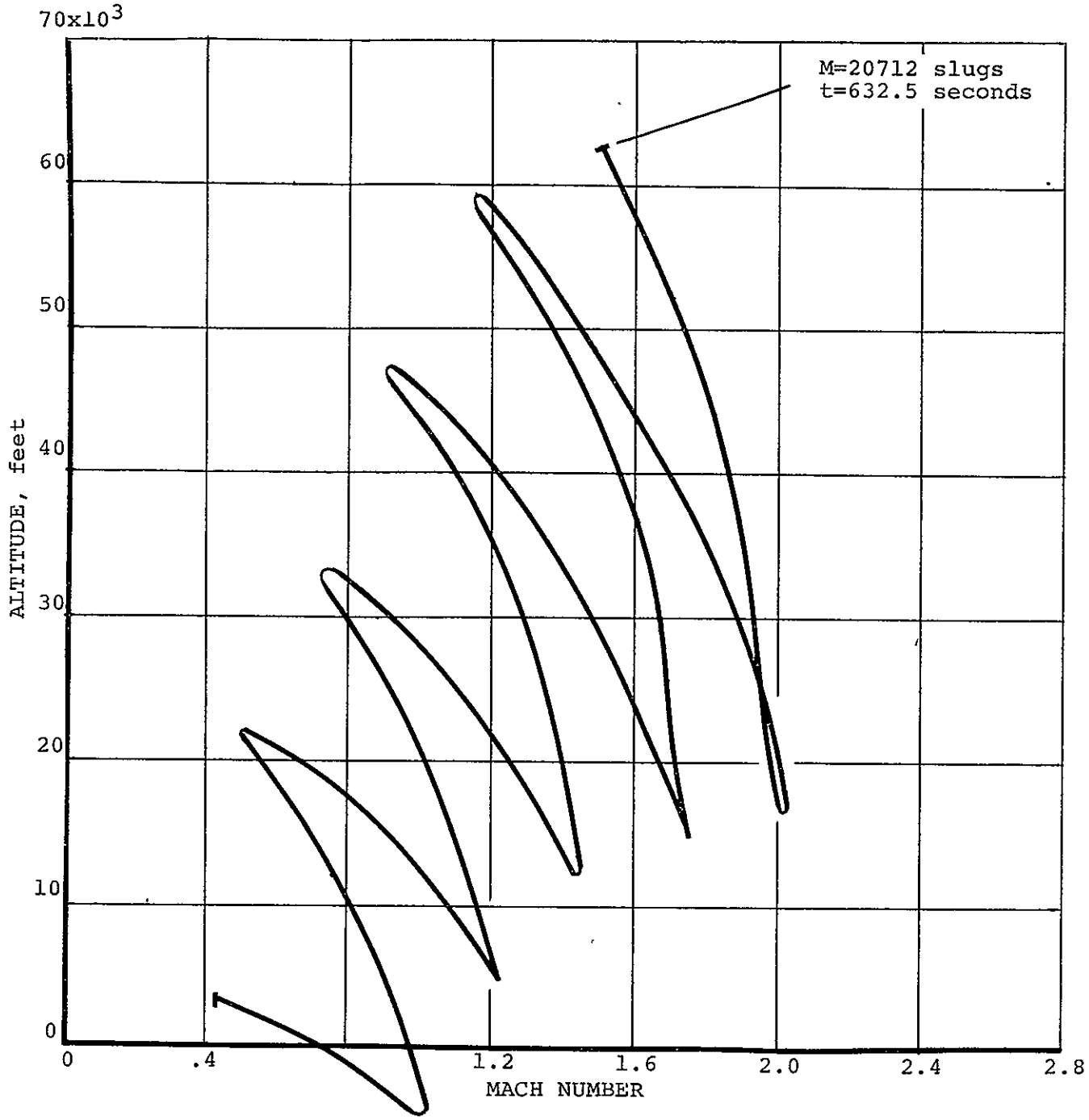

Figure 40.— Nominal Path, SST Maximum Mass Ascent
Angle-of-Attack Control

TABLE IX
CONVERGENCE DETAILS SST MAXIMUM MASS FULL THROTTLE ASCENT

ITERATION	MASS (SLUGS)	VELOCITY (ft./sec.)
0	20712	1448
1	20771	1389
2	20836	1333
3	20936	1213
4	21050	1008
5	21128	594
6	21174	710
7	21200	891
8	21171	1220
9	20916	1497
10	20905	1642
11	20895	1659
12	20660	1922
13	20628	1978
14	20353	2275
15	20344	2284
16	20340	2288
17	20042	2579
18	19778	2829
19	19995	2600
20	19990	2614
21	20014	2611
22	20020	2617
23	20021	2623
24	20061	2594
25	20046	2619
26	20051	2624
27	20053	2625
28	20064	2626

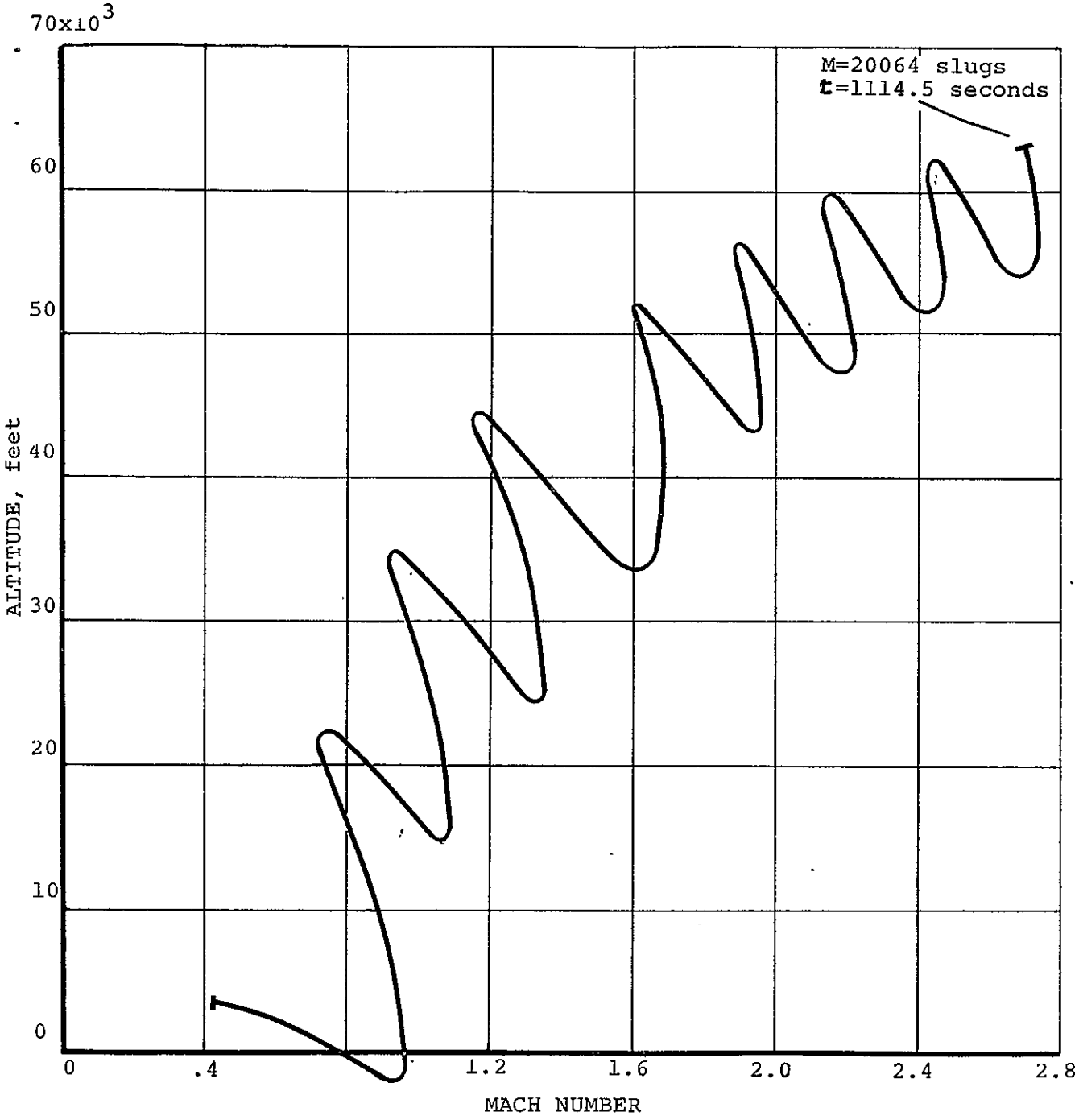

Figure 41.—Final Path, SST Maximum Mass Ascent Angle-of-Attack Control

M = 20064 slugs
R = 307.6 nautical miles

The final path of Figure 41 is a typical high lift long duration optimal path obtained with angle-of-attack control. The motion assumes a phugoid-like nature. A physical argument can be used to explain this type of path. If angle-of-attack and thrust were constant, phugoid motion would be produced. If these variables are almost constant, then phugoid-like motion will be produced. On a long duration path with smoothly changing control, then phugoid-like motions can readily develop. Such a path is nearly as efficient as smoother paths, and hence is retained in the steepest-descent process. The true non-oscillatory optimal path probably lies along the mean line through the phugoid-like path.

Piecewise Optimized Minimum Fuel Ascent, Angle-of-Attack Control

Piecewise optimization is often employed on long duration air-breathing vehicle trajectories. For example, the minimum time-to-climb flights of Reference 11 were obtained in this manner using the program of Reference 1. When piecewise optimization is employed, the trajectory is divided into a number of sub-arcs S^i. Performance and constraints, ϕ^i and ψ_j^i, are defined for each sub-arc, and the final state of S^i becomes the initial state for S^{i+1}. On the first arc the initial conditions for the complete mission are employed. On the final arc overall mission performance and constraints, ϕ and ψ_j are specified. Following piecewise optimization of a flight path, the optimized sub-arcs can be used to form a complete mission profile which, if desired, can be used as the nominal path for a complete trajectory optimization study. This step is often necessary, for the final set of sub-arcs obtained are, generally only sub-optimal from the overall mission standpoint.

For the SST minimum fuel ascent mission three sub-arcs are defined. The first sub-arc was defined as a maximum mass ascent to a Mach number of 1.2 at an altitude of 30,000 feet. Symbolically,

$$\phi^1 = M; \quad \psi_j^1 = M_N, h$$

Nominal and final paths obtained are included in Figure 42. A slight violation of the ground plane is present in this solution.

The objective of the study of this section was achievement of a smoother, possibly sub-optimal, ascent path to the SST cruise condition. Such a solution would hopefully cast light on the performance significance of the oscillatory SST ascent path obtained in the immediately preceding section. Accordingly on examination of the final path for the first sub-arc, the

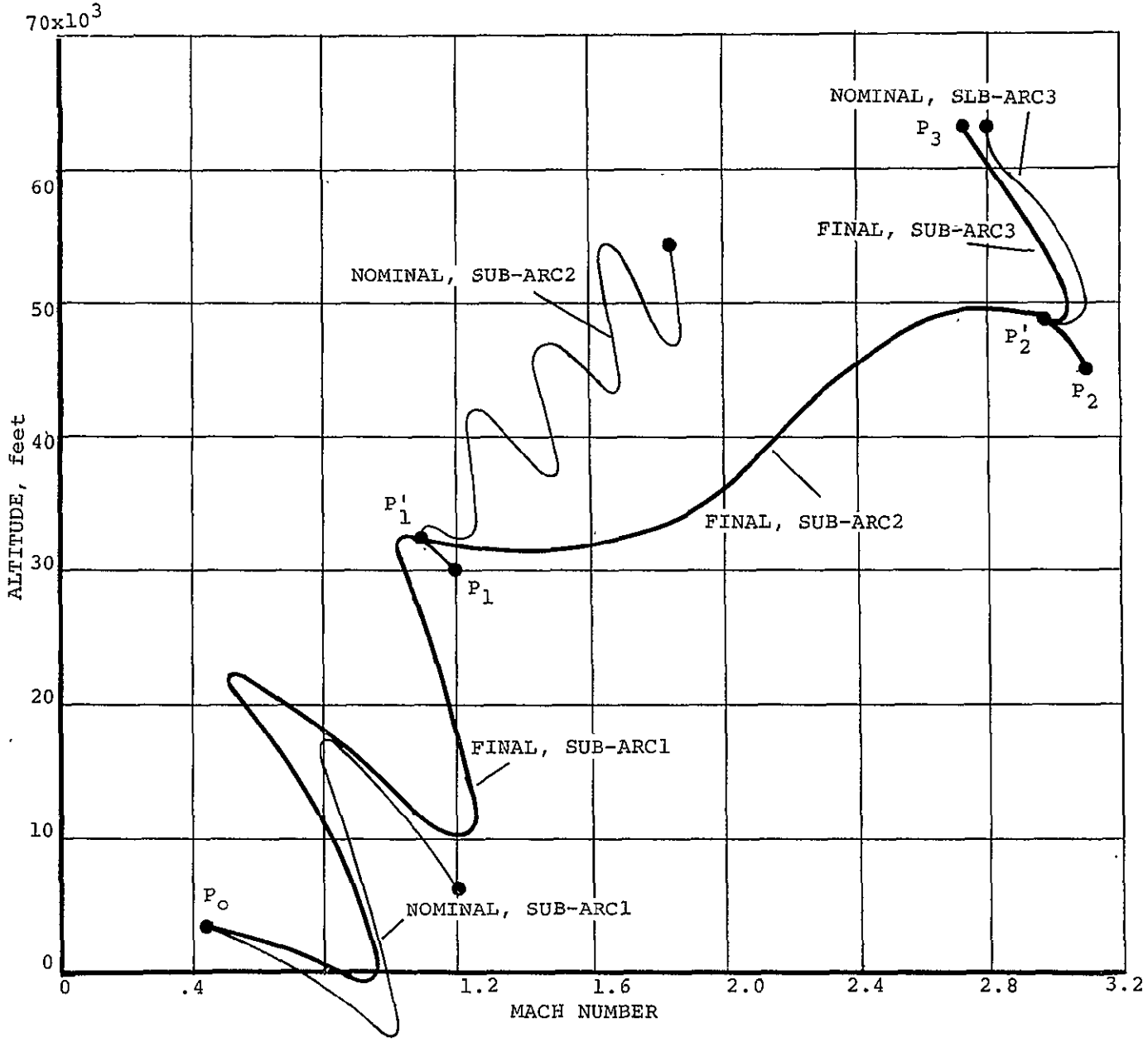

Figure 42.—Piecewise Optimized SST Ascent

point P_1' lying on the first sub-arc final path was selected as the initial condition for the second sub-arc.

The second sub-arc was defined as the maximum specific-energy path from the state at P_1' to a time of 700 seconds from P_o, an altitude of 45,000 feet, and with an inequality constraint $\gamma(t) \geq 0$ at all points on the flight path. This last constraint was intended to eliminate oscillatory motion in the SST supersonic sonic acceleration. Symbolically,

$$\phi^2 = E_{SP}; \quad \psi_j{}^2 = t, h, \gamma(t)$$

Initial state at the point P_1' was

t = 200 seconds
V = 1051 ft./sec.
h = 32052 feet
γ = 5.497 degrees
M = 21857 slugs
R = 32.4 nautical miles

The nominal path generated by a linearly varying angle-of-attack history is included in Figure 41 together with the final path obtained after twenty steepest-descent iterations, the sub-arc $P_1' P_2$. The final path obtained does not completely satisfy the flight path angle inequality constraint; nevertheless, oscillatory motion is practically absent from the supersonic acceleration. This result appears to demonstrate the effectiveness of the flight path inequality constraint

$$\gamma(t) \geq 0, \quad t_o \leq t \leq T$$

in elimination of the oscillatory motion associated with angle-of-attack control.

Following examination of the sub-arc $P_1' P_2$ the point P_2' lying on the arc was selected as the initial condition for a final arc defined as the maximum mass ascent to the SST cruise condition previously employed. Symbolically, for the third arc

$$\phi^3 = M; \quad \psi_j{}^3 = h, V, \gamma$$

The last constraint, $\gamma = 2°$, was imposed after a preliminary calculation without this constraint (not shown) resulted in a flight path angle in excess of 16 degrees.

Optimization of the last arc was rapid. Program termination on an internally defined optimum path occurred in 15 iterations requiring less than one minute per iteration. Initial state at P_2' was

t = 680 seconds

V = 2882 ft./sec.
h = 48509 feet
γ = -2.36 degrees
M = 20283 slugs
R = 160 nautical miles

Final state achieved at P_3 was

t = 708.6 seconds
V = 2625 ft./sec.
h = 63159 feet
γ = 1.93 degrees
M = 20208 slugs
R = 172 nautical miles

The piecewise optimization calculation which, as noted previously, is, at best, sub-optimal has utilized 2408 slugs of fuel in the ascent. This represents 10.6 per cent of the initial mass as compared with 11.3 per cent in the trajectory obtained in the preceding section. Time required for the two solutions differs by more than 400 seconds. It is evident from the convergence details presented in Table IX of the preceding section that the angle-of-attack control solution to the complete descent had not completely converged. Thus, the fuel discrepancy between the two solutions would ultimately be less than that quoted above.

Minimum Fuel Ascent, Pitch Angle Control

A final SST minimum fuel ascent was computed on the basis of pitch angle control. Initial conditions are identical to those of the two preceding sections. Therefore, final paths can be compared directly. Symbolically,

$$\phi = M; \quad \psi = h, V, \gamma; \quad \alpha = \theta(t)$$

A straightforward pitch control history, constant value of five degrees, generated the nominal path depicted in Figure 43. No trace of the oscillatory motion encountered with angle-of-attack control is apparent in this nominal path. Two points are worthy of note, however. First, some difficulty was experienced in locating a nominal pitch angle control history. Several earlier attempts to generate a nominal path using linearly varying pitch histories produced a condition of either too little or too much incidence ($\alpha = \theta - \gamma$) and the vehicle"pancaked." During the subsequent descents in a high drag attitude, the vehicle flight path integration became unstable. In consequence an integration step of $\Delta t = 2$ seconds was employed in place of the four-second step employed in the minimum fuel ascents using angle-of-attack control.

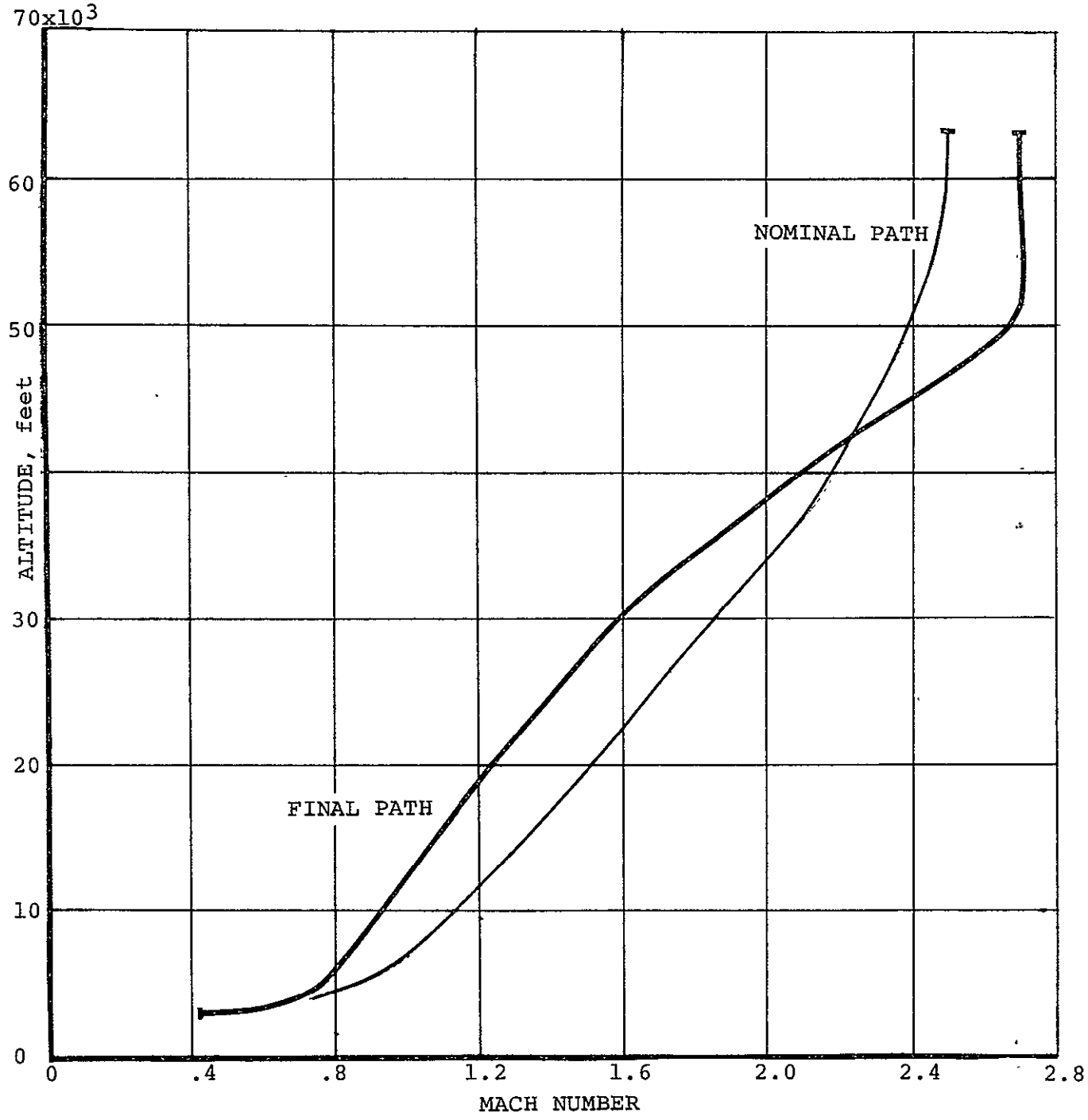

Figure 43.—Maximum Mass SST Ascent, Pitch-Angle Control

Following successful generation of the nominal, a very well-behaved convergence to the final path occurred. The final path obtained is included in Figure 43. Convergence details are presented in Table X. The final mass of 20425 indicates a fuel requirement of 2191 slugs, 9.7 per cent of the initial mass. This figure is an improvement over that obtained by angle-of-attack control (11.3 per cent) or piecewise optimization (10.6 per cent.) The final path is smooth, and there is no sign of the oscillatory motion encountered with angle-of-attack control. The performance improvement over that obtained by piecewise optimization could have been anticipated. The improvement over the angle-of-attack control result can be explained either as the result of a convergence failure or the result of the location of a second local extremal. From a physical viewpoint, the latter viewpoint seems likely; for it is possible that a subtle constraint has been imposed on the problem in the form of the number of phugoid-like oscillations. Thus, it might be that the angle-of-attack solution is the best path having eight oscillations, Figure 41.

Total flight time of the pitch control solution of Figure 43 is 631 seconds. This is less time than that taken by the piecewise optimization of the preceding section and almost half the time taken by the angle-of-attack solution. Complete final state of the pitch control solution is

$t = 631$ seconds
$V = 2620$ ft./sec.
$h = 63159$ feet
$\gamma = 0.3$ degrees
$M = 20425$ slugs
$R = 181$ nautical miles

It may be noted that the angle-of-attack solution attains a range well in excess of the above figure (307.6 nautical miles), a partial alleviation of its performance degradation. In fact, from the specific range aspect, the angle-of-attack solution is superior to the pitch control solution. This gain in specific range was fortuitous, of course, since range requirements were not included in the problem specification. It is clear, however, that future studies of SST climb performance capability should incorporate range requirements. For example, one might seek the path to $M = 2.7$, $h = 63000$ feet, $\gamma = 0$, and $R = 500$ nautical miles with minimum fuel consumption.

A final note on the SST minimum fuel ascents. True fuel minimization requires optimization of throttle history in addition to vehicle attitude. This optimization problem can be routinely studied with the program of Reference 1. Time constraints of the present study prohibited an investigation of this class of problems however.

TABLE X
CONVERGENT OF SST MINIMUM FUEL ASCENT, PITCH CONTROL

Iteration	Mass, slugs	Velocity,ft./sec.	Flight Path Angle
0	20392	2427	1.2°
1	20649	2290	3.4°
2	20659	2308	4.0°
3	20634	2357	3.6°
4	20603	2411	2.6°
5	20569	2464	1.6°
6	20530	2512	0.6°
7	20497	2545	0.1°
8	20425	2620	0.3°

REFERENCES

1. Hague, D. S.: Three-Degree-of-Freedom Problem Optimization Formulation - Analytical Development. Part I, vol. 3 FDL-TDR-64-1, McDonnell-Douglas Corporation, October 1964.

2. Mobley, R. L. and Vorwald, R. F.: Three-Degree-of-Freedom Optimization Formulation - User's Manual. Part II, vol.3, FDL-TDR-64-1, McDonnell-Douglas Corporation, October 1964.

3. Hague, D. S.: Atmospheric and Near Planet Trajectory Optimization by the Variational Steepest Descent Method. NASA CR 73365, 1969.

4. Hague, D. S. and Glatt, C. R.: An Introduction to Multivariable Search Techniques for Parameter Optimization (and Program AESOP). NASA CR73200, April 1968.

5. Hague, D. S. and Glatt, C. R.: A Guide to the Automated Engineering and Scientific Optimization Program - AESOP. NASA CR73201, April 1968.

6. Hague, D. S. and Glatt, C. R.: Application of Multivariable Search Techniques to the Optimal Design of Hypersonic Cruise Vehicle. NASA CR73202, April 1968.

7. Petersen, R. H., Gregory, T. J. and Smith, C. L.: Some Comparisons of Turboramjet-Powered Hypersonic Aircraft for Cruise and Boost Missions. Journal of Aircraft. Vol. 3, no. 5, September-October 1966.

8. Gregory, T. J., Petersen, R. H. and Wyss, J. A.: Performance Trade-Offs and Research Problems for Hypersonic Transports. Journal of Aircraft. Vol. 2, no. 4, July-August 1965.

9. Raybould, B.: Approximate Trajectories for Maximum Range. Journal of the Royal Aeronautical Society. June 1963.

10. Hague, D. S. and Glatt, C. R.: Study of Navigation and Guidance of Launch Vehicles Having a Cruise Capability. Vol. 2, Boeing doc. D2-113016-5, The Boeing Company, 1967.

11. Landgraf, S. K.: Some Practical Applications of Performance Optimization Techniques to High-Performance Aircraft. AIAA Paper 64-288, July 1964.

APPENDIX - PROGRAM MODIFICATIONS

Several of the problems solved in the study required modification of the Reference 1 program. Modification of tabular data functional dependency or in the amount of space allocated to each table were required. These modifications are a routine part of program operation and, hence, will not be discussed further. Two modifications involving program computational flow were undertaken in the study and are discussed briefly below.

Drag-Brake Modification

The minimum range HRA trajectories contained in the body of this report were performed with drag brakes fully extended. The resulting Mach-dependent drag increment is shown in Figure 44. Addition of this drag increment to the vehicle aerodynamic input would have required fairly extensive changes to vehicle data. Accordingly, an alternative procedure was followed. The drag increment was treated as a negative thrust utilizing the propulsive characteristics. Figure 44 illustrates the programmed revision to the vehicle thrust and fuel flow subroutine TFFS. Figure 44 should be compared to the TFFS program flow diagram on Page 60 of Reference 2. With the modification the positive drag increment is placed in table TTAB10 as a function of Mach number, angle-of-attack, altitude, and throttle setting. In the present case, the Mach number dependency was the only variation employed. Zero fuel flow was specified in TTAB11. The basic program safeguard on negative thrust was eliminated in this version of TFFS. It may be noted that the dependency of incremental drag on "throttle setting" could be used in optimizaton studies.

Pitch-Angle Control

Air breathing vehicle trajectories are often more readily solved when pitch-angle is employed in place of angle-of-attack. A modification permitting the use of pitch-angle was introduced into the program of Reference 1 during the study. The modification is limited to one macro-statement in the differential equations of motion subroutine DIFEQ. The macro-statement involved is FNCUVW, Page 35, Reference 2. The modification is illustrated in Figure 45. On entering FNCUVW, the angle-of-attack is computed as the difference between pitch-angle and flight path angle. Angle-of-attack is then employed in determination of the body-axis to wind-axis rotation matrix, $[u,v,w]$ and in the aerodynamic subroutine SACS. Following this, pitch-angle is reset to the sum of angle-of-attack and flight path angle.

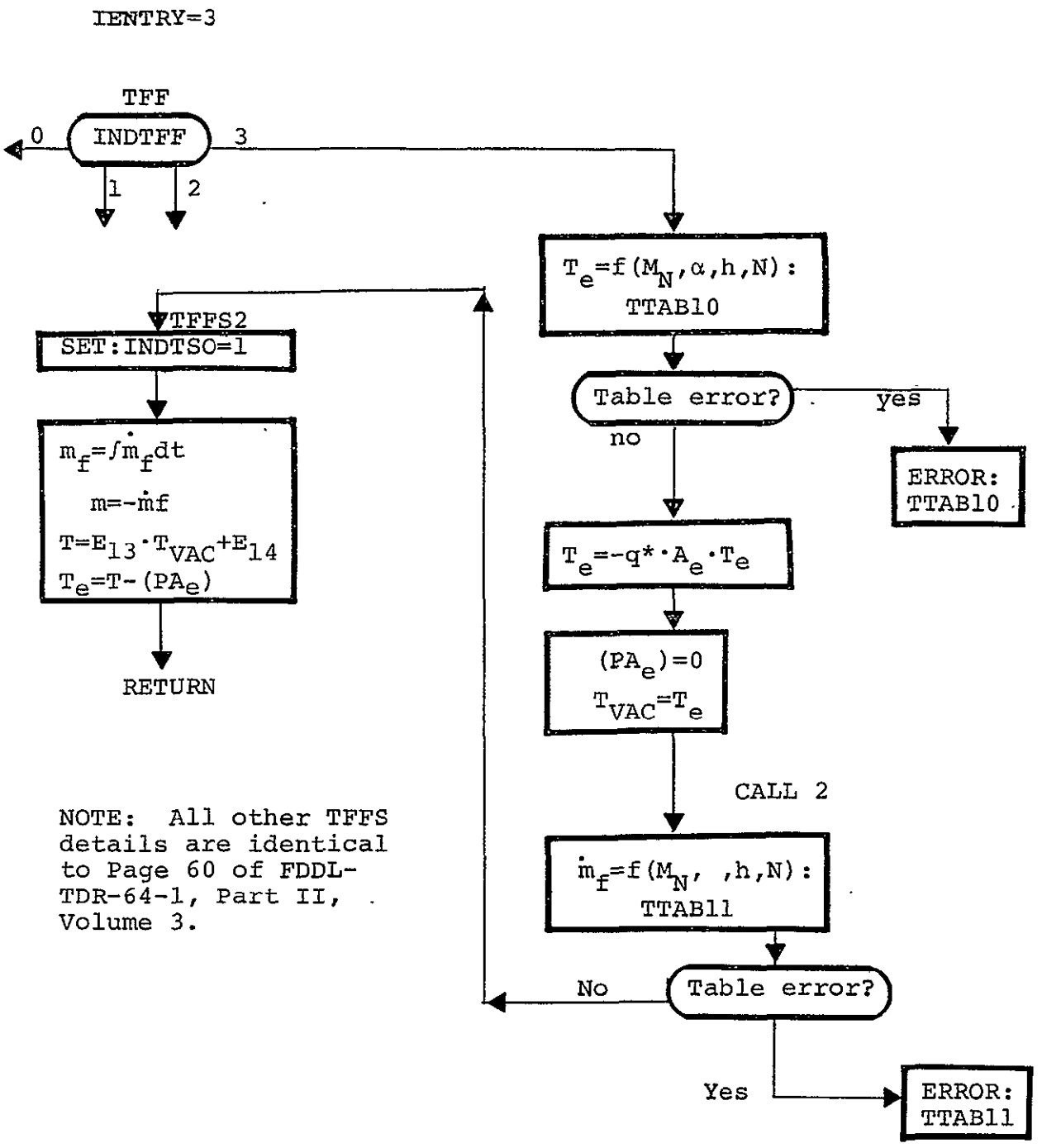

Figure 44.-Speed Brake Modification To TFFS

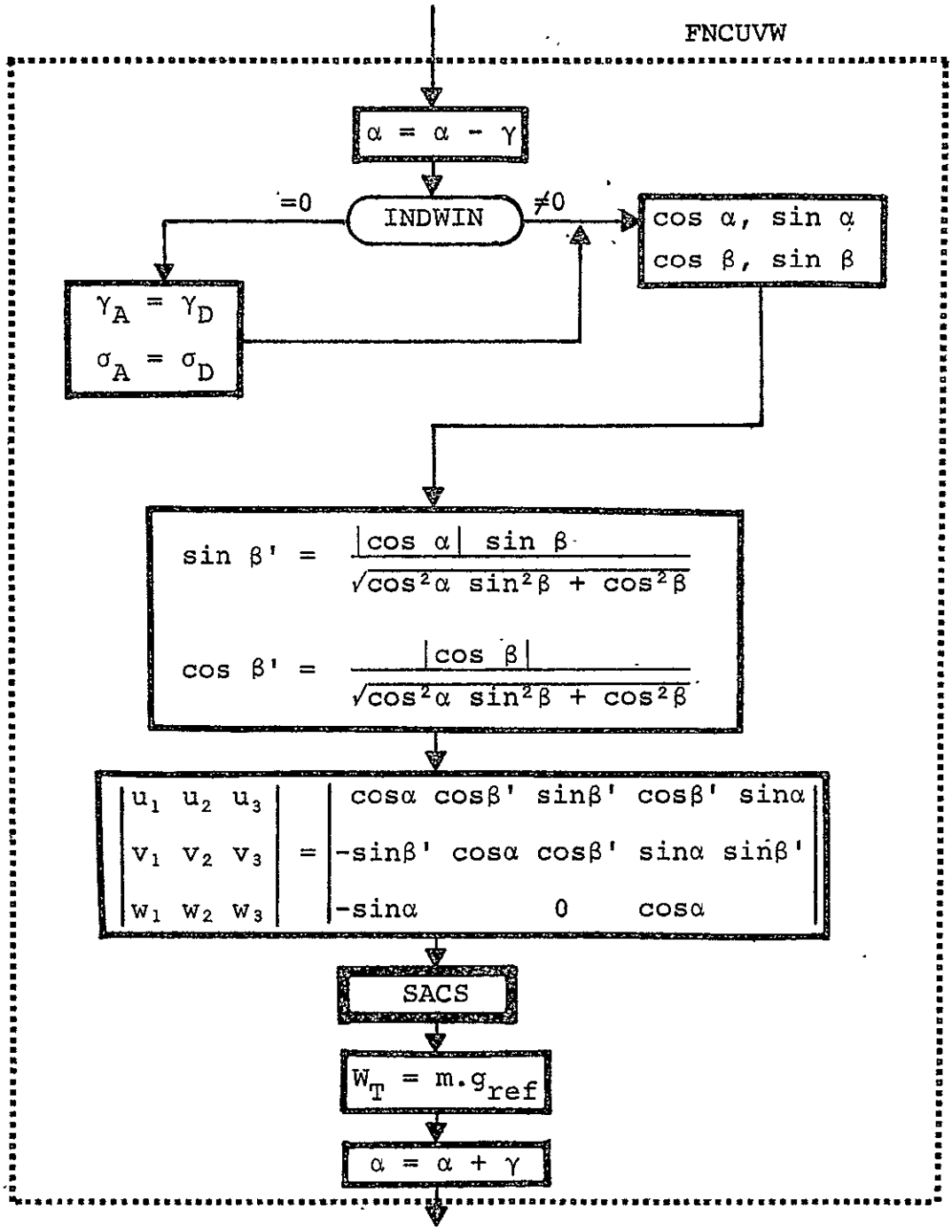

Figure 45-Pitch Angle Control Modification, DIFEQ

It should be noted that in non-planar motion, the above definition of pitch-angle is incorrect. In fact, the "pitch angle" employed then becomes the algebraic sum of flight path angle and total angle-of-attack provided a coordinated turn is employed.